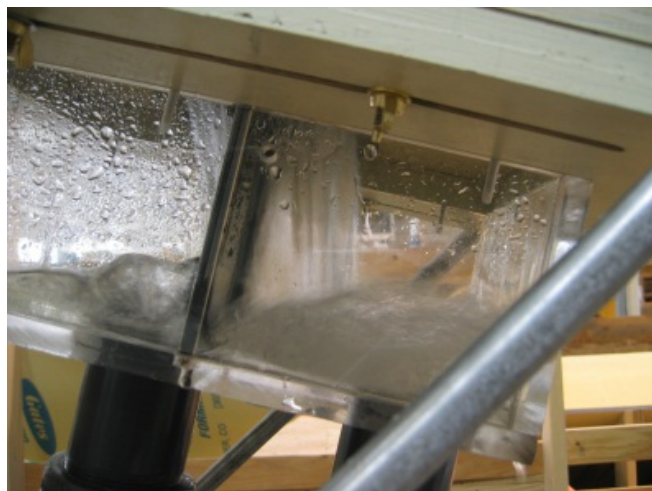# RECLAMATION
Managing Water in the West

Improving Coanda-Effect Screen Technology

Research and Development Office
Science and Technology Program
Final Report ST-2017-6295-01
Hydraulic Laboratory Report HL-2017-08

Mission Statements

Protecting America's Great Outdoors and Powering Our Future

The Department of the Interior protects and manages the Nation's natural resources and cultural heritage; provides scientific and other information about those resources; and honors its trust responsibilities or special commitments to American Indians, Alaska Natives, and affiliated island communities.

REPORT DOCUMENTATION PAGE			*Form Approved* *OMB No. 0704-0188*
1. REPORT DATE: SEPTEMBER 2017	**2. REPORT TYPE:** RESEARCH		**3. DATES COVERED**
4. TITLE AND SUBTITLE Improving Coanda-Effect Screen Technology			**5a. CONTRACT NUMBER** XXXR4524KS-RR4888FARD160120001 (8)
			5b. GRANT NUMBER
			5c. PROGRAM ELEMENT NUMBER 1541 (S&T)
6. AUTHOR(S) Tony L. Wahl			**5d. PROJECT NUMBER** ST-2017-6295-01
			5e. TASK NUMBER
			5f. WORK UNIT NUMBER 86-68560
7. PERFORMING ORGANIZATION NAME(S) AND ADDRESS(ES) Hydraulic Investigations and Laboratory Services Group (86-68560) U.S. Department of the Interior, Bureau of Reclamation, PO Box 25007, Denver CO 80225-0007			**8. PERFORMING ORGANIZATION REPORT NUMBER** HL-2017-08
9. SPONSORING / MONITORING AGENCY NAME(S) AND ADDRESS(ES) Research and Development Office U.S. Department of the Interior, Bureau of Reclamation, PO Box 25007, Denver CO 80225-0007			**10. SPONSOR/MONITOR'S ACRONYM(S)** **R&D:** Research & Development Office **BOR/USBR:** Bureau of Reclamation **DOI:** Department of the Interior
			11. SPONSOR/MONITOR'S REPORT NUMBER(S) ST-2017-6295-01
12. DISTRIBUTION / AVAILABILITY STATEMENT **Final report can be downloaded from Reclamation's website: https://www.usbr.gov/research/**			
13. SUPPLEMENTARY NOTES			

14. ABSTRACT *(Maximum 200 words)*
Coanda-effect screen structures provide high capacity removal of coarse and fine debris from water intakes, such as small hydropower installations, irrigation diversions, and storm water runoff facilities. The screens are hydraulically self-cleaning, making them well suited to remote sites without electrical power. Flume tests of prototype screen materials were performed to measure screen discharge coefficients, which were then related to dimensionless parameters of the flow. The most recent testing has investigated a wider range of flow conditions than previous work, which has led to the development of new discharge equations. Performance of the screens is demonstrated to be dependent on a combination of inertial, gravitational, and surface tension forces that can be quantified with the Froude number and Weber number. Screen performance is shown to be independent of the Reynolds number (viscous forces).

15. SUBJECT TERMS water screens, fish screens, screening, Coanda effect, surface tension, Reynolds number, scale effects

16. SECURITY CLASSIFICATION OF:			**17. LIMITATION OF ABSTRACT** U	**18. NUMBER OF PAGES** 48	**19a. NAME OF RESPONSIBLE PERSON** Tony Wahl
a. REPORT U	**b. ABSTRACT** U	**c. THIS PAGE** U			**19b. TELEPHONE NUMBER** 303-445-2155

S Standard Form 298 (Rev. 8/98)
P Prescribed by ANSI Std. 239-18

Improving Coanda-Effect Screen Technology

Prepared by: Tony L. Wahl
Hydraulic Engineer, Hydraulic Investigations & Laboratory Services Group, 86-68560

Technical Approval: Robert Einhellig, P.E.
Manager, Hydraulic Investigations & Laboratory Services Group, 86-68560

Peer Review: Bryan Heiner, P.E.
Hydraulic Engineer, Hydraulic Investigations & Laboratory Services Group, 86-68560

Acknowledgments

Executive Summary

Water intakes of all kinds require the separation of debris, fish, sediment, and other matter from water. The need for effective debris separation systems has increased in recent years as the removal of debris on a finer scale becomes necessary. In irrigation, modern water application techniques (e.g., drip, sprinklers, gated pipe) require removal of debris at a finer scale than traditional flood irrigation. For small-scale hydropower facilities, fish, sediment, and fine debris removal are needed at remote sites. For storm water runoff facilities extensive and distributed fine debris removal solutions are needed to comply with increasingly stringent water quality standards.

Coanda-effect screens offer a solution to many of these screening problems. These structures combine high-capacity screening, self-cleaning hydraulic performance, and fine debris removal, all driven by gravity with no need for electrical power. Reclamation research in the 1990s developed methods for estimating flow capacity of these screens, but did not consider the full range of flow conditions for which they could be applied today.

To enable Coanda-effect screen use in a wider range of flows than originally intended (specifically at low velocities on flatter inclines when there is little available head drop), new testing of several screen materials was performed in a flume with a slope that was adjustable from nearly horizontal to an incline of over 50°. This testing led to the development of new discharge equations that will be used to improve predictions of the flow capacity of field-scale structures.

The new testing demonstrated that screen capacity is a complex function of both the Froude number and Weber number. These dimensionless flow parameters indicate the relative contribution of inertial (mass of the water), gravitational (slope of the screen and depth of flow), and surface tension forces. Previous work had also identified some of these factors, but did not test a wide enough range of conditions to accurately predict screen capacity in some important real-world situations. The new testing also definitively showed that the Reynolds number (ratio of viscous to inertial forces) does not have a significant effect on screen flow capacity. Because water viscosity varies significantly with temperature, this means that screen performance should be largely independent of water temperature (until temperatures drop low enough to form ice).

The new test results have dramatically reduced the uncertainty of predictions of discharge through these screens, with errors in flow prediction reduced from about ±50% to ±10%. The new discharge coefficient model will especially improve the accuracy of flow predictions for structures that utilize screens installed on relatively flat slopes and with low head drop. This will broaden the potential range of application for Coanda-effect screens.

Three areas for continued research were identified as a result of this study:

- Aerated flow in the receiving chamber below the screen panel should be studied so that screen structures can be designed to avoid unexpected effects of aeration.
- Flow skipping was observed on a few screens with large tilt angles when operating at high flow velocities, steep slopes, and shallow flow depths (i.e., large Froude numbers).

This causes the Coanda effect to be lost, allowing water to detach from screen wires and skip over the screen instead of flowing through it. Testing is needed to develop criteria for predicting the onset of flow skipping so that it can be avoided in prototype structures.

- Although Coanda-effect screens are generally self-cleaning, the hydraulic self-cleaning action is not always sufficient to prevent some types of debris from clinging to the screen surface and eventually building up to a point that restricts flow. Research is needed to develop criteria for flow conditions and debris types that lead to a loss of self-cleaning action. It would also be valuable to perform research to develop methods for improving self-cleaning action.

Contents

Tables

Figures

Introduction

On water resources projects around the world it is necessary to separate a wide variety of foreign objects from water used for municipal, industrial, energy production and agricultural purposes. Coanda-effect screens offer promise to meet this need with several practical advantages over more traditional debris screening methods. These include an ability to remove very fine (small) debris, a relatively large flow capacity per unit screen area, and a self-cleaning hydraulic action that keeps screens clean without mechanical cleaners or other moving parts.

Coanda-effect screens have been utilized worldwide since the 1980s for high capacity screening of organic debris, trash, sediment, and aquatic organisms from a variety of water intakes (Finch and Strong 1983; Strong and Ott 1988). Fontein (1965) also described the use of a similar screen for solids removal in mining applications as early as 1955. In the late 1990s the Bureau of Reclamation conducted hydraulic testing that led to the development of computer software for predicting the flow capacity of Coanda-effect screens and designing structures to meet site-specific discharge objectives (Wahl 2001). More recently, Esmond (2012) described the use of Coanda-effect screens for applications related to storm water management, and May (2015) conducted laboratory tests to evaluate the effectiveness of the screens for sediment removal at municipal water intakes.
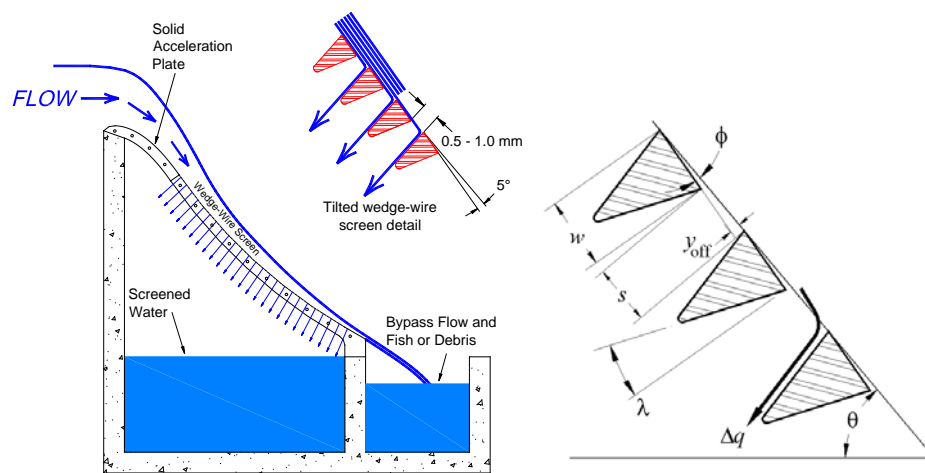
Figure 1. — Typical arrangement of a Coanda-effect screen structure and definition of geometric variables for screen materials.

A typical Coanda-effect screen structure is shown schematically in Figure 1 (Wahl 2001). The screen panel is installed downstream from the crest of an overflow weir so that high-velocity flow passes across the screen surface. An acceleration plate leads flow tangentially onto the screen. The screen panel is composed of wedge wire oriented perpendicular to the flow direction. Each wire is tilted a few degrees downstream on its axis so that the leading edges of the wires form a series of water-shearing offsets projecting into the flow. The Coanda effect allows flow to attach to the top surface of each wire so that the flow in the immediate vicinity of the wires is parallel to the top surfaces of the wires. At the trailing edge of each wire the flow detaches cleanly from the wire, and upon striking the face of the next downstream wire a thin layer of water is turned and discharged through the slot between the wires. Coanda-effect

screens do require a significant drop of head for satisfactory performance, and this has been a significant impediment to their widespread use.

Flow conditions over the full length of a screen panel vary considerably. To enable the customized design of screen structures, Reclamation has previously performed two series of tests of small, prototype screen material specimens in fixed-slope flumes (Wahl 2001) and in a variable-slope flume over a limited range of incline angles (Wahl 2013). The previous work showed that screen capacity was a function of the slot width, screen porosity, wire tilt angle, Froude number (Fr), Reynolds number (Re), and Weber number (We). (Specific definitions for each of these parameters are provided in the Experimental Program section.)

In these earlier works, the discharge through each screen slot was modeled mathematically by considering the flow through the screen surface to be the combined result of the shearing action of the wire offsets and the orifice capacity of the slots due to the pressure head of the flow above the screen surface. The discharge equation was based on a virtual flow velocity vector combining the actual velocity parallel to the screen surface and a theoretical velocity component perpendicular to the screen surface, derived from the conversion of the pressure head of the flow into velocity head. Wahl (2001) related the associated discharge coefficient to the Froude number and the ratio of viscous to surface tension forces (Re/We). Wahl (2013) used the same definition for the discharge coefficient, but related it to a flow angle of attack that can also be directly related back to the Froude number. Unfortunately, neither previous work provided experimental data to validate the relation at Froude numbers less than about 4, and most data were collected at only two incline angles, 15° and 37°. Since low Froude numbers do occur at the top (upstream end) of prototype screen structures (just downstream from the acceleration plate) and over extended areas of screens with relatively flat incline angles, it is important to understand this flow condition well to make good predictions of total screen performance.

Experimental Program

To evaluate screen performance over the wide range of flow conditions encountered in practice, a new series of tests was conducted using the test facility further adapted from that described by Wahl (2013). Several previously tested screen specimens were tested again over a wider range of flow conditions, at slopes ranging from $\theta = 1°$ to 50° below horizontal (see Figure 1). Previous testing showed that screen discharge coefficients were a function of three dimensionless flow parameters, the Froude number, the Reynolds number, and the Weber number, defined as follows:

$$\mathsf{Fr} = \frac{V}{\sqrt{gD \cos \theta}} \tag{1}$$

$$\mathsf{Re} = \mathsf{Re}_{\mathrm{slot}} = \frac{Vs}{\nu} \tag{2}$$

$$\mathsf{We} = \mathsf{We}_{\mathrm{offset}} = \frac{\rho V^2 y_{\mathrm{off}}}{\sigma} \tag{3}$$

where:

V = flow velocity above the screen surface,
g = acceleration due to gravity,
D = flow depth above the screen surface,
θ = screen incline angle below horizontal,
s = slot width of the screen,
ν = kinematic viscosity of the fluid,
ρ = fluid density,
y_{off} = height of the offset created by the wire tilt, and
σ = surface tension coefficient of the fluid.

The dimensionless parameters Fr, Re, and We represent the ratios of inertial to gravitational forces, inertial to viscous forces, and inertial to surface tension forces, respectively.

To isolate the effects of each parameter, ideally testing would be conducted so that each parameter was varied independently while the others were held fixed. However, the most convenient way to organize the majority of the testing was to set a fixed flume slope for each test and operate the facility at varying discharges (and velocities), which meant that in any single test run, all three dimensionless parameters were varying at the same time. To overcome this challenge, one screen was tested with the water temperature varied while flow rates and flume slopes were held constant. This allowed the Reynolds number to be varied almost independently from the Weber number while the Froude number was held nearly constant.

Test Facility

A unique 0.15-m (6-inch) wide adjustable-slope flume was constructed in the hydraulics laboratory of the Bureau of Reclamation to determine screen throughput under a range of hydraulic conditions. The facility is similar to the fixed-slope flume used for studies reported in Wahl (2001), but with greater flexibility to perform testing over a broad range of flow conditions. The facility is described in detail in Wahl (2013). Figure 2 and Figure 3 show components of the test facility, including the head tank, the flume with three available screen test locations (top, middle, and bottom, each 0.38 m = 15 inches apart), two V-notch weirs for measurement of screened flows, and a tailwater tank. Flow rates up to 442 L/min (0.26 ft^3/s) can be recirculated through the head tank and flume. By varying screen positions, flume slopes, and flow rates, a wide range of flow conditions can be produced.

The objective of the testing is to determine the discharge capacity of screen slots located in the midst of a relatively long length of prototype screen, but the first few slots are known to accept flow less efficiently. This is thought to be due to the fact that the flow has not yet become fully aligned to the top surface of the screen wires, but may also be due to the boundary layer that develops on the flume section leading to the screen. This boundary layer is gradually removed as flow passes through the screen, so that in the midst of a screen there is little to no boundary layer, which was verified in the tests by Wahl (2001). To create a mid-screen flow condition at

the test section, flow through the most upstream slots of each tested screen (about one third to one half of the screen specimen length, adjustable) was collected and measured, but considered wasted, while the flow through the downstream slots was also collected and measured to provide the test result. For the flow over the "test" portion of the screen, the flow depth, velocity, and dimensionless flow parameters were computed at the upstream and downstream ends of the test section to determine average values at the midpoint of the test section. Flow depths and velocities above the screen surface were not specifically measured, since previous testing showed that they could be calculated analytically knowing the discharge through the flume and the headwater level measured in the head tank.

Discharges into the flume were measured with a transit-time acoustic flow meter, and the entrance to the top of the flume was calibrated during the early phases of the testing to enable the inflow to also be determined from a head-discharge relationship. Flows through the upstream and downstream sections of the test screen were determined by collecting each flow stream in a weir box and measuring the collected flows using custom-made V-notch weirs that were calibrated in-place using time-volume measurements. The test facility as described here was first established in the hydraulics laboratory in 2012; in early 2016 it was moved to a new location in the laboratory and was equipped there with a larger tailwater tank and new V-notch weir measurement boxes, but remained functionally similar to the 2012 facility.

Figure 2. — Screen test facility.

Figure 3. — Screen installed in the flume and the collection box beneath the flume.

Screens

Table 1 shows the physical properties of all of the tested screens. All wire tilt angles were measured using the optical reflection method described in Wahl (2001). Wire and slot widths were measured using calipers at several locations over the surface of each screen. The reported

13

relief angles for each wire shape are the designated values given by screen manufacturers for each wire shape. The majority of the reported dimensions match those given in previous references, but the wire tilt angles for screens A-5, A-8, B-1, and B-2 were adjusted slightly from the values reported in Wahl (2013) based on new measurements.

Table 1. — Properties of tested screens.

Screen	A-5	A-8	B-1	B-2	#1	#2	#3
Relief angle, λ, degrees	10	10	13	13	17.5	12.5	11
Wire tilt angle, ϕ, degrees	5.6	6.0	4.3	6.5	3.82	3.57	6.88
Avg. slot width, s, mm	1.99	1.96	2.05	2.05	1.02	0.99	0.47
Avg. wire thickness, w, mm	4.72	4.74	4.60	4.62	2.39	1.55	1.50
Offset height, y_{off}, mm	0.652	0.800	0.498	0.753	0.227	0.158	0.233
Specimen width, mm	76	76	89	89	93	104	87
Specimen length, mm	79	79	89	89	76	72	73
Specimen length, slots	11	11	13	13	22	40	36
Support bar spacing, mm	54	54	51	52	70	19	13.5
Support bars	9.5-mm round	9.5-mm round	6.4-mm square	6.4-mm square	9.5-mm round	4.0-mm round	4.0-mm round

A custom mounting block was constructed for each screen to allow it to be mounted flush with the flume surface. Custom divider plates were also built to divide the upstream waste section of the screen and the downstream test section. The divider plates fit snugly beneath the screen surface and the support bars, and modeling clay was used to further ensure a watertight seal between the two screen sections during testing. Figure 4 shows one of the tested screens installed into its mounting block.

Figure 4. — Test screen B-1 in mounting block and a view of the underside of the screen with divider plate installed. Flow is left to right in both photos.

Analysis

The previous research efforts at Reclamation led to the development of a conceptual model used to mathematically describe the flow condition at an individual screen slot and compute a discharge coefficient for flow through the slot. During the course of the present study, much of the early data analysis utilized this model, but it was ultimately shown that the model could not adequately represent the performance of the screens over the wider range of flow conditions considered for this study (Wahl et al. 2017). As a result, a new conceptual model was developed. Details of the original model are not repeated here, but can be found in Wahl (2001) and Wahl (2013). The new conceptual model is described below and is used for the majority of the data analysis provided in this report.

Discharge Equation

The discharge equation adopted for this study is based on the screen geometry shown in Figure 5. The tilted-wire construction causes the screens to remove a thin layer of water from the bottom of the water column and direct it out the bottom of the screen. The velocity of water across the screen face is V and this velocity is presumed to remain constant as the flow is turned. Conceptually, the unit discharge through the screen at each wire is

$$\Delta q = V \cdot y_{\text{off}} \tag{4}$$

where y_{off} is the thickness of the water layer removed by the raised offset. This equation assumes several idealized properties for the flow situation:

- The flow across the screen is attached to and parallel to the upper surface of each wire and cleanly detaches without any change of flow direction so that it is directed straight into the face of the next downstream wire (no gravitational deflection of the jet), where it is turned with 100% efficiency through the screen.
- The velocity profile is uniform (no significant boundary layer) and is represented by the free-stream velocity of the flow over the screen, V.
- The thickness of the diverted flow stream is equal to $y_{\text{off}} = (s + w \cos \phi)\sin \phi$, or for small values of ϕ, $y_{\text{off}} = (w + s)\phi$
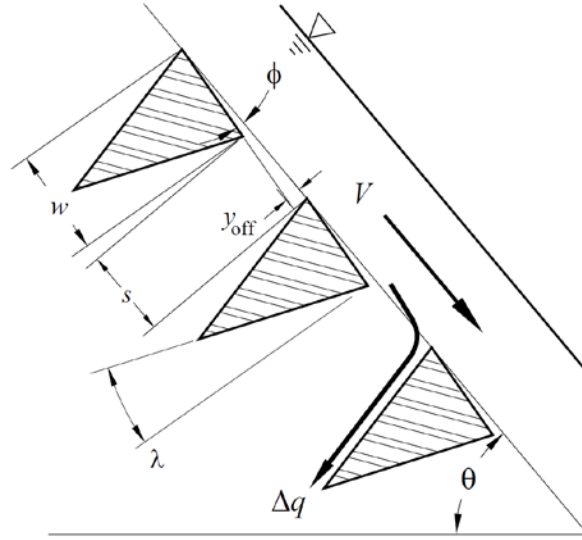
Figure 5. — Screen geometry and flow variables.

In reality, none of these assumptions are perfect, so a discharge coefficient is introduced:

$$\Delta q = C_{\text{offset}} \cdot V \cdot y_{\text{off}} \tag{5}$$

In particular, it is expected that as flow depth above the screen increases, the thickness of the water layer removed by each wire may exceed the offset height and may instead approach the slot width, s. Discharge coefficients greater than 1.0 should be expected in this case.

Testing and Results

Evaluation of Edge Effects

Before proceeding with the presentation of test results, two questions must be addressed regarding width or edge effects in these studies. Since relatively narrow screen samples are being tested, two different edge effects are possible. The first is the effect of the support bars that lay beneath the triangular profile wire screen elements. Testing by Wahl (2001) established that flow control occurs at the screen surface, so discharge performance of Coanda-effect screens is independent of the support bar spacing. The second possible edge effect is due to the width of the test flume compared to the width of the test screen. Since all of the tested screens are narrower than the flume width, it seems possible that the flume width to screen width ratio could significantly affect the geometry of flow streamlines as they approach and pass through the screen slot openings.

To address the possibility of this second effect, a series of tests were run using screens #1 (at a 5.1° flume slope) and A-5 (at a 26.3° slope), with variable widths of the screen left open to the flow (Figure 6). A full range of flow rates was run over each screen, and the tests showed that discharge coefficients were unaffected by the variable width of the screens for flume to screen width ratios in the range of 4.57 down to 2.28 (Figure 6). This was encouraging, but the design of the test facility does not make it practical to run a physical test in which the screen is the same

width as the flume, and any facility designed to allow that would potentially have edge effects from the no-slip condition that must exist at the flume walls. Thus, there was still a question whether an edge effect would be seen for smaller flume to screen width ratios. Finally, this question was resolved when a computational fluid dynamics (CFD) model was constructed and run by a Ph.D. student who visited the Reclamation laboratory in August of 2016. This model showed no significant edge effects down to width ratios of 1:1 (Dzafo et al. 2017).

Production Testing

The screens shown in Table 1 were tested extensively from 2012 to 2017 at a wide range of incline angles, from as flat as 1° to as steep as 50°, and at top, bottom, and middle positions in the flume. Testing in 2016 and 2017 included a full range of slopes, especially very flat and very steep slopes, and mostly at the top and bottom screen positions. Data were collected in 2012 primarily at slopes of 15° and 30° using all three screen positions. Slopes up to 60° are typical in field installations, but physical limits of the apparatus made it logistically difficult to test at slopes steeper than 50°. The flume slope was determined by the use of a digital level that recorded slope in degrees and percent. For each run, slope measurements were made from both the right and left sides of the flume and the average slope value was recorded.
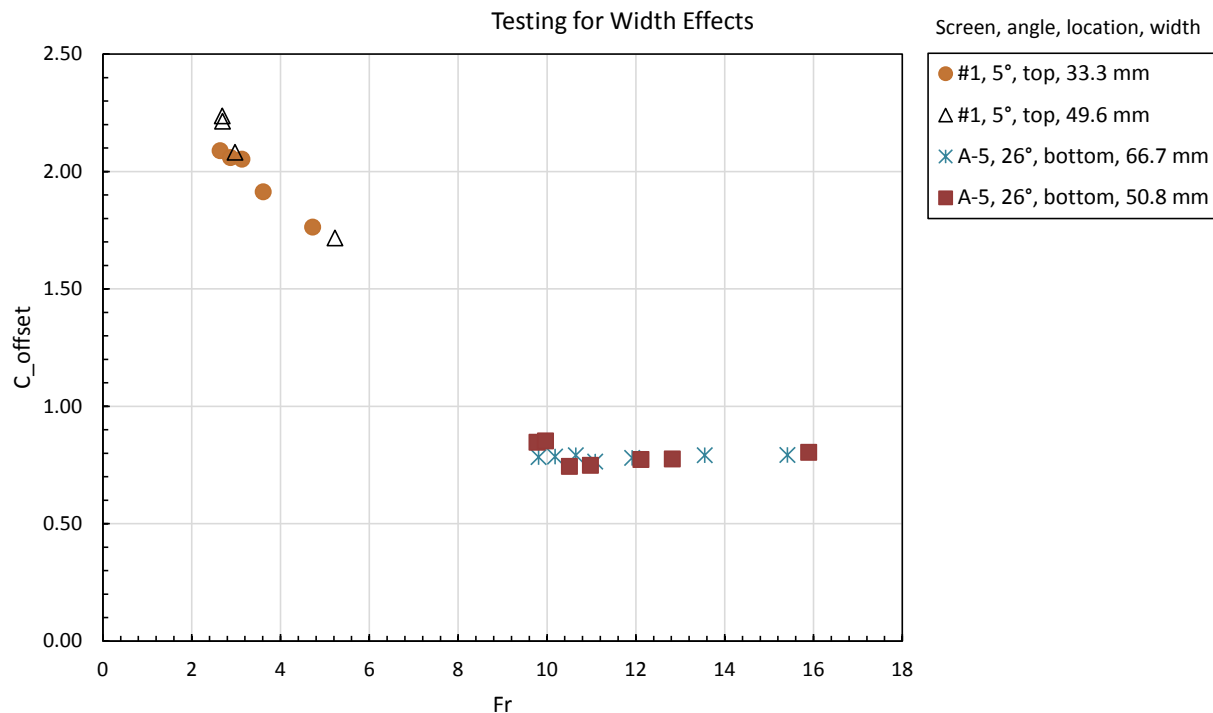

Figure 6. — Data showing no effect of changing the width of the screen exposed to the flow.

A few screens with large tilt angles (exceeding 7°) were tested at steep slopes and at the bottom position in the flume and exhibited skipping of the flow, indicating loss of the Coanda effect (attachment of the flow to the top surface of the wire). The flow would detach from the leading edge of individual wires and skip over downstream wires, reducing screened discharge significantly. Particular wires with a large tilt angle or a slight offset above the plane of the

screen would tend to always be the first to skip as the flow velocity was increased or as flow depth over the screen decreased. When skipping occurred it was very easily observed visually. Flow skipping did not affect any of the test data reported here. Although flow skipping was associated with the combination of large wire tilt angles, steep slopes, high flow velocities, and shallow flow depths (i.e., large Froude numbers), no attempt was made in this study to develop specific criteria for predicting when flow skipping would occur. Figure 7 shows examples of normal flow and skipping flow.

For each test, the flume was operated first at the maximum discharge of the pump (about 0.25 ft^3/s = 110 GPM = 6.94 L/s) and then at gradually lower discharges until there was little to no flow depth on the toe of the screen. For each run, the flow rate into the flume was determined either from an ultrasonic flow meter or from a measurement of water surface elevation in the head tank supplying the flume. As testing proceeded, data were collected to build a rating curve for the entrance to the flume (standard error 1.6%) so that data collection gradually shifted to recording only the head tank water elevation. Similarly, water levels were recorded for the two V-notch weir boxes receiving flow from the waste and test sections of the flumes, and in early tests, flows were also measured from these weirs by timing the collection of the weir outflow in a 4 L graduated cylinder. Again, these data were used to create in-place calibration curves for the 30° V-notch weirs so that data collection in later stages of the project could be accomplished solely by recording water levels. Standard errors for the waste-flow and test-flow V-notch weirs were 3.4% and 2.1%, respectively.
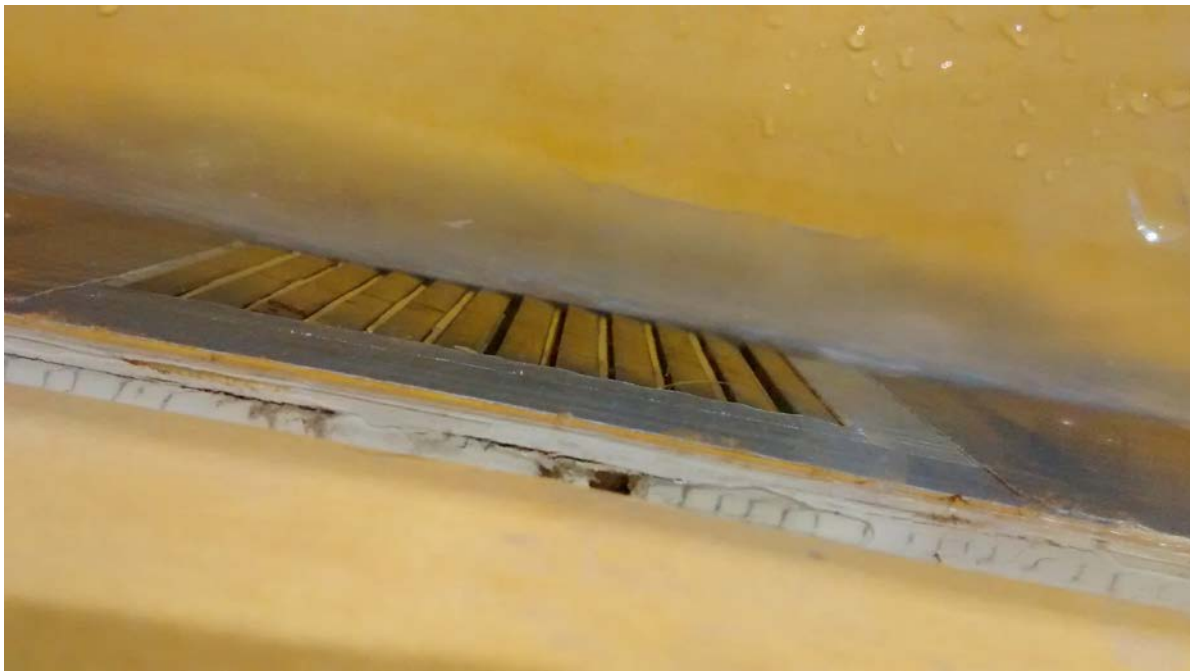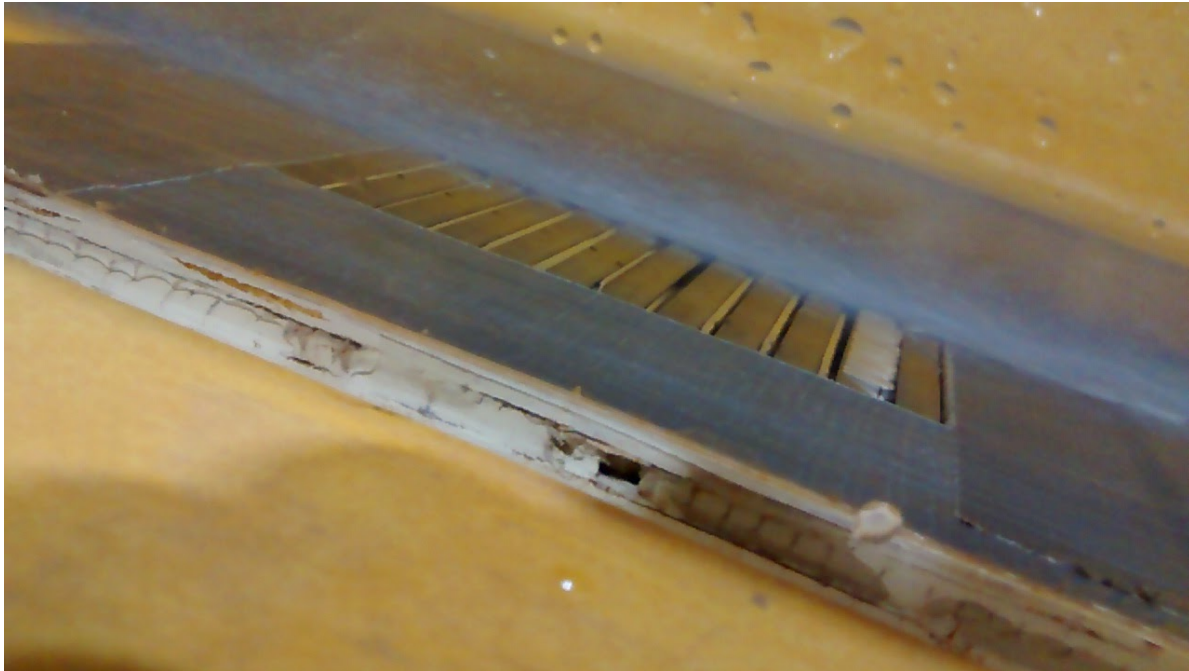
Figure 7. — Normal flow through screen A-8 (top) and flow skipping over one wire of screen A-6 (bottom). Screen A-6 is similar to A-5 and A-8, but with a measured wire tilt of 7.5°. Flow is left to right in both images.

For each screen test position (top, middle, or bottom) the flow distance and elevation drop from the crest to the start of the screen could be determined based on the flume slope and the geometry of the flume crest. Knowing the discharge into the flume, a flow profile was calculated from the crest (where critical depth was assumed) to the start of the screen. This profile assumed a Manning's n value of 0.009 for the crest (a circular arc section of a PVC pipe) and the flume (marine plywood on the floor and the left wall, and clear acrylic on the right wall). This roughness value had been previously determined to produce an accurate estimate of the flow velocity at the start of the screen, based on Pitot tube measurements performed for earlier studies. To determine flow conditions at the downstream end of the waste section of the screen (and upstream end of the test section), a flow profile was calculated across the waste section for spatially varied flow with decreasing discharge, with the flow exiting through the screen at each slot determined from the measured flow through the associated V-notch weir. This screened flow was assumed to be evenly distributed through the waste slots. Similarly, a gradually varied flow profile calculation was made over the test section of the screen to determine the flow conditions at the downstream end of the test section. Depth, velocity, Froude, Reynolds, and Weber numbers were calculated for the upstream and downstream ends of the test section, and average values were determined. These average values were used to develop correlations between flow parameters and the observed screened flow and calculated discharge coefficients.

Initial analysis of the collected data was attempted using the same discharge equation used in Wahl (2001) and Wahl (2013). Discharge coefficients for that model (C_{cv}) were calculated from the measured flow data and the observed values were compared to values predicted using previously developed equations (Figure 8). Neither method adequately predicted values of C_{cv} over the wide range of test conditions, with errors as large as ±50% (Figure 8).

Test results were ultimately analyzed using the new discharge equation (Eq. 5). Values of C_{offset} were determined from the experiments and plotted against the Froude number (Eq. 1), Reynolds number (Eq. 2), and Weber number (Eq. 3). The Froude number used here is adjusted for channel slope by inclusion of the $\cos(\theta)$ term, as presented in Chow (1959). The energy coefficient, α, which is often included in the Froude number, was assumed equal to unity. The Reynolds and Weber numbers both utilize the free-stream velocity across the screen as their velocity reference. Consideration was given to several different length references for these parameters, and ultimately the most satisfying relationships were developed using the wire offset height, y_{off}, (the nominal thickness of the sheared water layer) for the Weber number and the slot width, s, for the Reynolds number.

When discharge coefficient values were plotted versus each dimensionless number, initially a relation to each parameter could be demonstrated (Figure 9 and Figure 10), and the form of each relation appeared to be primarily an inverse relation, with discharge coefficients decreasing as Fr, Re, and We increased. However, the fact that all three parameters seemed to have a significant influence and were all varying simultaneously during the tests made it difficult to isolate the influence of each. In fact, it was suspected that some of the correlations were spurious since all of the dimensionless numbers vary to some degree with one another (all being proportional to the flow velocity).
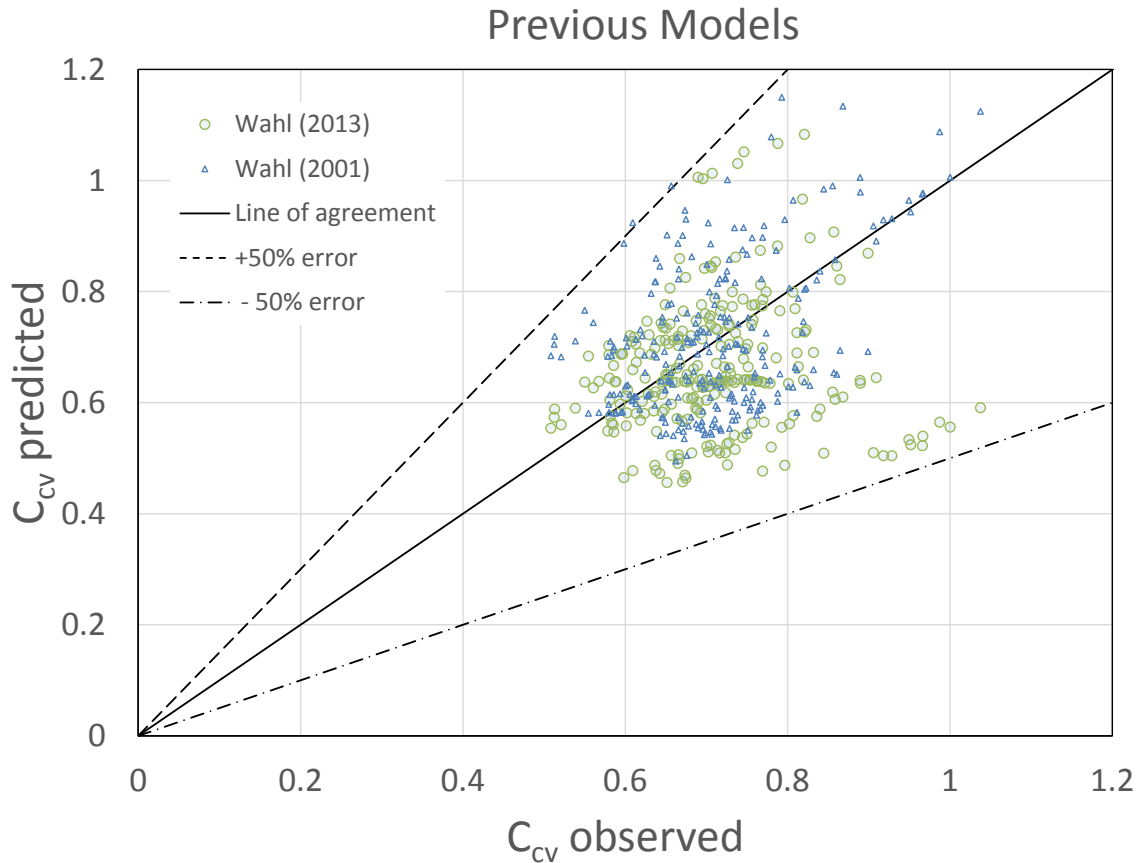

Figure 8. — Predictions of screen discharge coefficients with previously developed models.

To investigate the potential for spurious correlations, data were filtered in an attempt to isolate the effects of varying only one parameter. Figure 11 shows data collected from screen #1 over a wide range of Froude numbers and a narrow band of Reynolds and Weber numbers. (Data from only screen #1 are shown for clarity, but similar behavior can be seen in data from other screens.) Figure 12 shows slices of data from a wide range of Reynolds and Weber numbers with a narrow band of Froude numbers. Unfortunately, for any single screen it is not possible hold a constant Reynolds number while varying the Weber number or vice versa, so it is not possible to determine whether the relations shown in Figure 12 represent distinct Reynolds and Weber number effects, or similar effects that are spuriously correlated with one another.
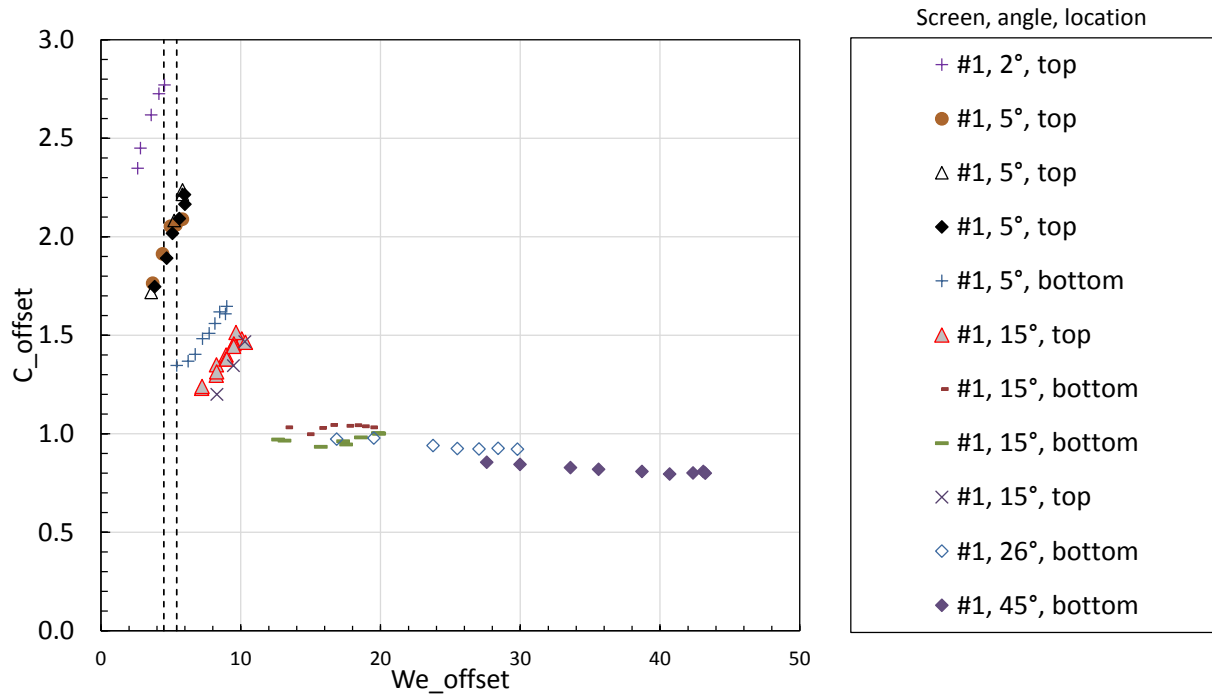
Figure 9. — Relation of C_{offset} to Weber number for screen #1.

(a) **(b)**
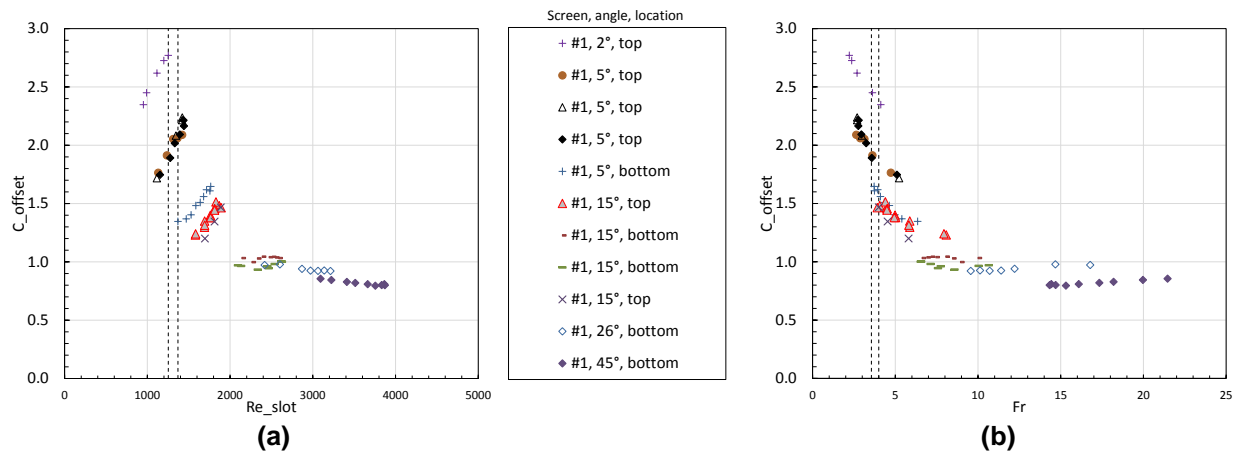
Figure 10. — Relations between C_{offset} and (a) Reynolds number and (b) Froude number.
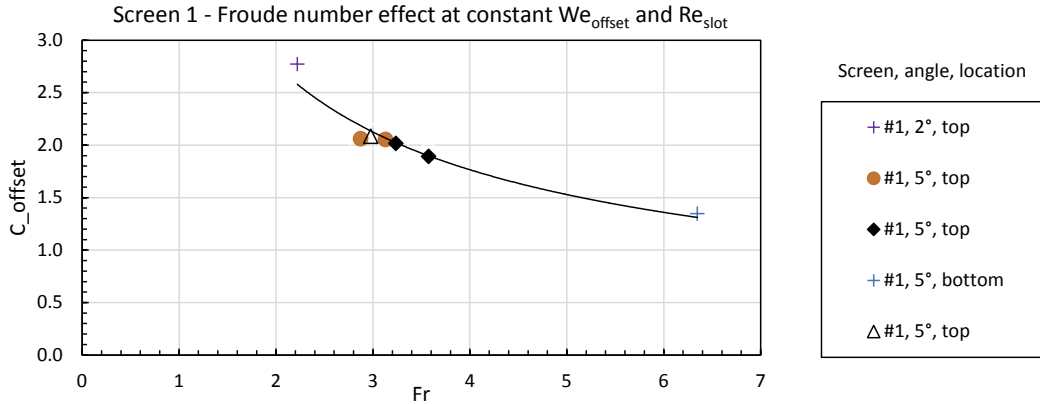
21

Figure 11. — The Froude number effect is illustrated by filtering data from screen #1 to show values at nearly constant Weber and Reynolds numbers. The range of We_{offset} is 4.50 to 5.41 and the range of Re_{slot} is 1253 to 1370 [vertical slices in Figure 9 and Figure 10(a)].
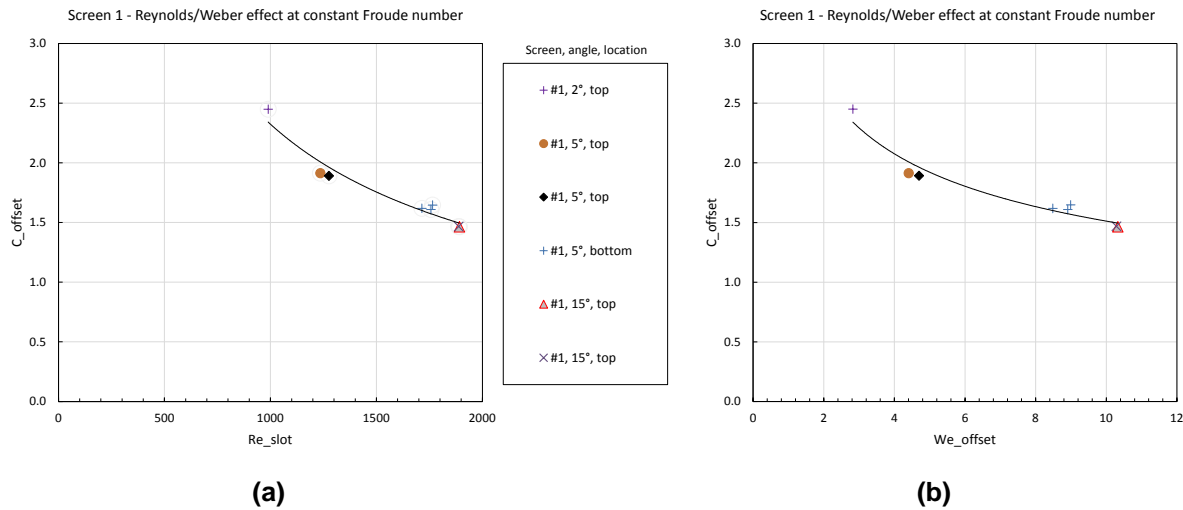

(a)   **(b)**

Figure 12. — Reynolds and/or Weber number effects are illustrated by filtering data from screen #1 to show values at nearly constant Froude numbers (3.55 to 4.0) within the vertical slice indicated in Figure 10(b).

Variable-Temperature Tests

To isolate the effects of the Reynolds and Weber numbers, a series of tests of screen #1 were performed in which the water in the test facility was gradually chilled (from about 70°F to near 37°F) while a constant discharge was delivered to the test screen at a fixed flume slope and test position. Water viscosity increases about 60% over this temperature range, but the surface tension coefficient increases by only about 3%, so this provides a way to observe Reynolds number effects independently from Weber number effects. Additionally, testing was repeated at three different flume slopes and discharges, which provided data points with different Weber numbers and nearly matching Froude and Reynolds numbers.

Figure 13 shows that there was no Reynolds number effect when the water temperature was varied. The data set collected at the middle slope (14.6°) suggested a slight trend, but it was not statistically significant. Figure 14 shows the Weber number effect
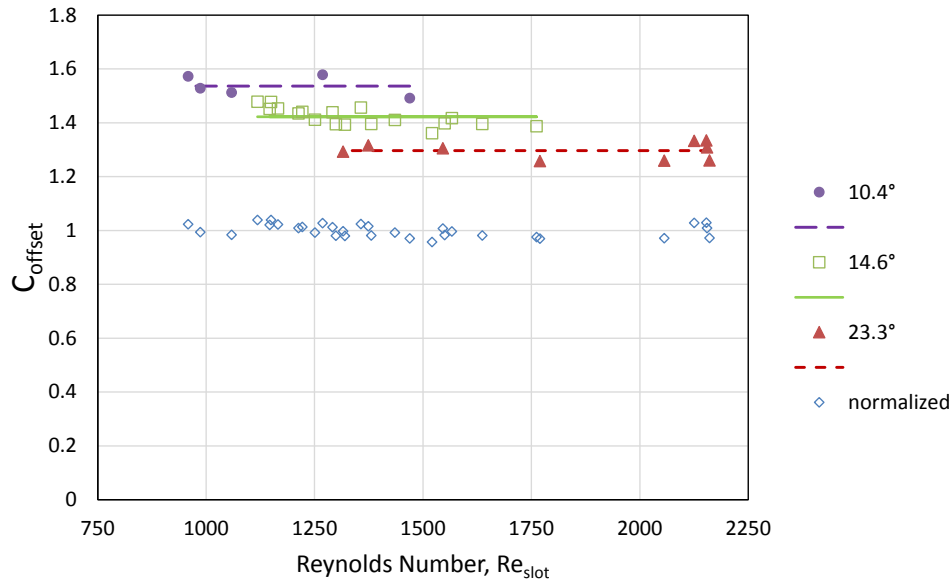
22

Figure 13. — Variable temperature tests show that there is no Reynolds number effect on the discharge coefficient. All of the data sets have the same Froude number. Each data set has a different, fixed Weber number. The combined data set is normalized about each of the respective averages to remove the Weber number effect.

Length Reference for Weber Number

Following the variable-temperature tests, it was apparent that the Reynolds number could be neglected in further analysis. The remaining question was what length reference should be used to define the Weber number. Although the offset height, y_{off}, was used for early analysis of screen #1, it still seemed plausible that the slot width, wire width, or flow depth could also serve as useful length references. To examine this question, discharge coefficients were plotted versus Weber numbers constructed using each of these length references. The Weber number based on flow depth exhibited no useful relationship, but Weber numbers based on the offset height, slot width, and wire width all exhibited strong inverse relationships to the discharge coefficient.

Several pairs of screens offered the potential for determining which Weber number might be the most useful for describing all of the data. Screens B-1 and B-2 were similar in all of their properties except for small differences in the wire tilt angle and resulting offset height, as were screens A-5 and A-8. Screens #1 and #2 had similar slot widths (approx. 1 mm) and wire tilts (about 3.8° and 3.6°), but much different wire widths and thus significantly different offset heights. Screens #1 and #3 had similar offset heights despite significantly different wire widths (2.39 mm and 1.50 mm) and slot widths (1.02 mm and 0.47 mm). Figure 15 compares observed discharge coefficients to Weber numbers defined with different length references for each of these screen pairings. For screens B-1 vs. B-2 and A-5 vs. A-8 the comparison is inconclusive; A-5 and A-8, which have a little larger difference in offset heights, show a poorer collapse of the data when the offset height is used as the length reference. The comparison of screens #1 and #2 suggests that the offset height and wire width are both effective length references, and this result seems encouraging, since these screens had significantly different values of both of these parameters. The comparison of screens #1 and #3 suggests the offset height is the best length

23

reference; these screens had significantly different wire widths and slot widths, and the use of these lengths references failed to effectively collapse the data. Although this analysis suggests the offset height as the most suitable length reference for the Weber number, it must also be kept in mind that Froude number effects also play a significant role, and screens with different offset heights will have much different Weber numbers at similar Froude numbers and vice versa. Finally, later analysis shows that screens #3 and A-8 performed differently from the other five screens for unexplained reasons, so it is difficult to draw conclusions from comparisons involving them. Ultimately, the ability to construct an effective model for predicting the discharge coefficient as a function of Fr and We should be used to judge which Weber number most effectively describes the data.
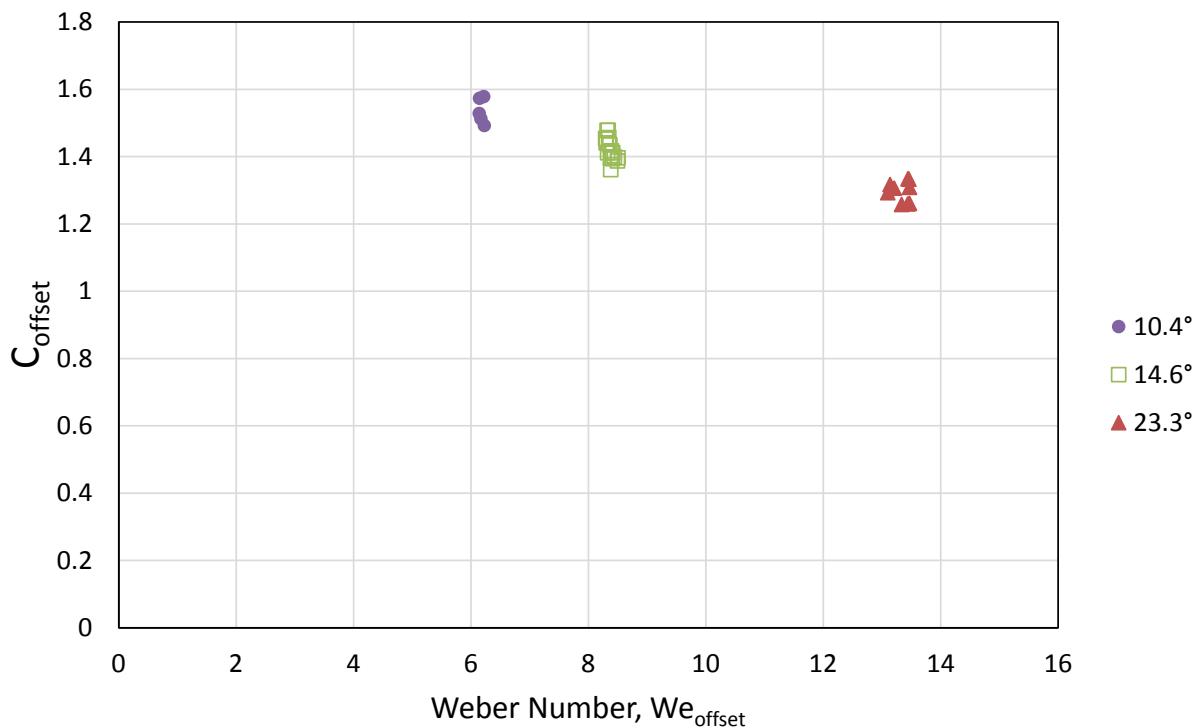
Figure 14. — The Weber number (surface tension) effect is clearly demonstrated in tests run with nearly constant Froude numbers (5.09 to 5.28) at three different Weber numbers. The trend is similar to that seen in Figure 12 for a slightly lower range of Froude numbers.
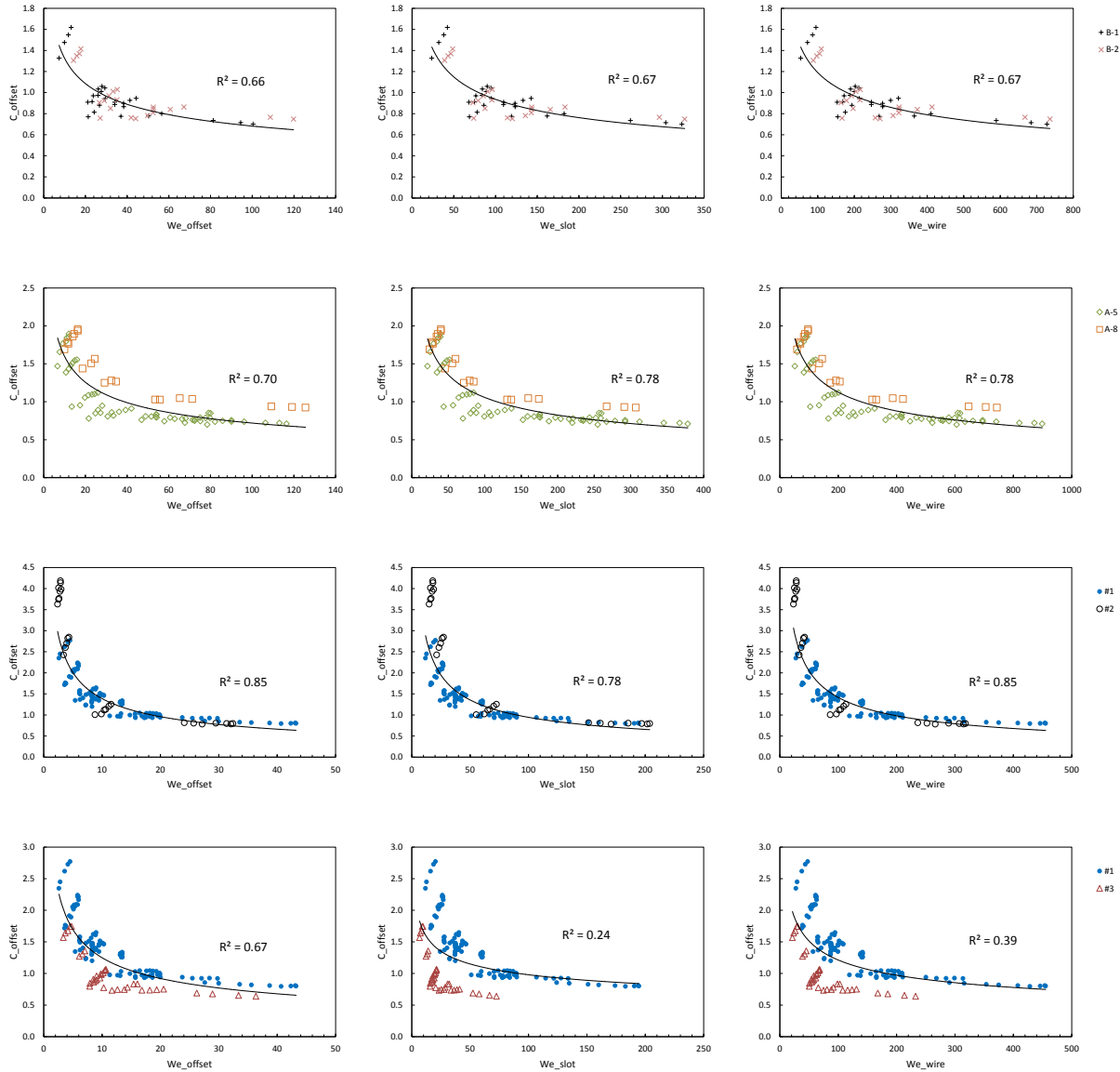
Figure 15. — Comparison of different Weber numbers to observed discharge coefficients of four pairs of screens: B-1 and B-2 (top row); A-5 and A-8 (second row); #1 and #2 (third row); #1 and #3 (bottom row).

Discharge Coefficient Prediction Equation

Figure 10 previously showed that discharge coefficients appeared to be inversely related to both the Weber number and Froude number, but it is not immediately apparent what function would most effectively model this relation. Two likely possibilities were a power curve or exponential function of either the Weber number or Froude number, with the coefficients perhaps modified by functions based on flow parameters or screen properties. A series of equations was tested for data sets collected from single screens and for combined data sets comprising multiple screens. Values of best-fit numerical parameters in the equations were determined using the Excel Solver. Ultimately, the most successful curve fits were obtained with an equation of the form:

$$C_{\text{offset}} = \left(a + b\frac{2}{2 + \text{Fr}^2}\right)(\text{We}_{\text{offset}})^{c \cdot \text{Fr}^d} \tag{6}$$

with a, b, c, and d being curve-fitted numerical constants. Equations utilizing the Froude number at the heart of the power curve equation (in the position of $\text{We}_{\text{offset}}$) were far less effective at fitting the data. Equations based on Weber numbers utilizing the slot width and wire width were effective for single screens, but less effective when applied to multiple screens. Table 2 shows optimized values of the coefficients for individual screens and for several groupings of screens, and the associated root mean square values of the percentage error in the predicted C_{offset} value. It should be noted that all screens can be modeled well when curve fitting is performed individually (RMS errors of 7% or lower), and several grouped sets of screens are modeled well (RMS errors below 10%), but when screens #3 and A-8 are included in any group, RMS errors increase substantially. These two screens perform significantly different from all others, for reasons that cannot be fully explained. Screen #3 accepts significantly less water than would be expected based on its measured geometric properties, and screen A-8 takes in more water than expected. Screen dimensions and wire tilt angles were double-checked, but nothing was found that would account for the performance differences. It is possible that these screens perform differently due to imperceptible differences in the sharpness of the leading edges of the wires compared to the other tested screens.

Table 2. — Coefficients of Eq. 6 and curve-fitting results.

Screen	a	b	c	d	Average error	RMS error
#1	0.941	20.516	-1.533	-1.096	-0.21 %	4.54 %
#2	0.826	25.055	-1.542	-1.150	-0.08 %	2.90 %
#3	0.752	8.242	-0.741	-0.946	-0.07 %	2.65 %
A-5	0.967	10.863	-0.586	-0.741	-0.35 %	5.94 %
A-8	1.112	14.009	-0.801	-1.008	-0.09 %	2.93 %
B-1	0.885	12.832	-0.927	-0.981	-0.44 %	6.64 %
B-2	0.949	7.605	-0.458	-0.748	-0.37 %	6.11 %
#1, #2	0.959	24.915	-1.689	-1.041	-0.34 %	5.84 %
#1, #2, #3	0.914	25.276	-2.106	-1.091	-2.66 %	16.30 %
A-5, A-8	0.875	9.661	-0.491	-0.838	-1.15 %	10.75 %
B-1, B-2	0.915	10.701	-0.739	-0.911	-0.43 %	6.53 %
A-5, B-1, B-2	0.952	11.228	-0.671	-0.811	-0.41 %	6.42 %
#1, #2, A-5	1.031	21.283	-1.206	-0.887	-0.45 %	6.73 %
#1, #2, A-8	0.908	16.853	-0.987	-1.024	-0.70 %	8.35 %
#1, #2, A-5, B-1, B-2	1.031	21.174	-1.210	-0.888	-0.48 %	6.94 %
#1, #2, A-5, A-8, B-1, B-2	1.030	19.302	-1.056	-0.860	-0.80 %	8.96 %
#1, #2, #3, A-5, B-1, B-2	0.918	15.463	-1.076	-0.963	-2.03 %	14.23 %
All screens	0.916	13.764	-0.881	-0.922	-2.25 %	14.99 %

The observation that screens have variable individual performance characteristics suggests that laboratory testing should be performed whenever the most accurate predictions of screen discharge are needed. However, five of the seven screens tested here performed similarly and

can be adequately modeled by Eq. 6 using the shaded coefficients shown in Table 2. When testing cannot be performed on a specific screen, these coefficients can be adopted as default values to be used until testing can be conducted to verify screen performance. Appendix A provides four plots for each tested screen. The plots show the variation of observed values of C_{offset} compared to Fr and We$_{offset}$, and also the predictions of C_{offset} made using Eq. 6. Predictions are plotted for the optimized coefficients of each individual screen and for the suggested default coefficients.

The ratio $2/(2+Fr^2)$ proved to be more effective than the raw Froude number in the multiplier term of Eq. 6. This ratio was shown in Wahl (2001) to be the fraction of the flow specific energy associated with flow depth, while its complement $Fr^2/(2+Fr^2)$ represents the kinetic energy fraction. Either ratio could be used; the curve-fitted coefficients a and b will adjust as needed. This ratio was also considered for use in the term that provides the exponent for We, but a power curve of the raw Froude number was more effective. An equation utilizing a constant exponent (replacing the $c{\cdot}Fr^d$ term) was also developed, but was much less effective when fitting to data from multiple screens.

Figure 16 demonstrates the fit of Eq. 6 to the observed discharge coefficients for screen #1. Observed values are overlaid with predicted values and the equation explains most of the variation of the observed values. Figure 17 shows the ability of Eq. 6 to predict discharge coefficients for screens #1, #2, A-5, B-1, and B-2, using the default parameters shaded in Table 2. Comparing this back to Figure 8 shows dramatic improvement of the accuracy of flow predictions.
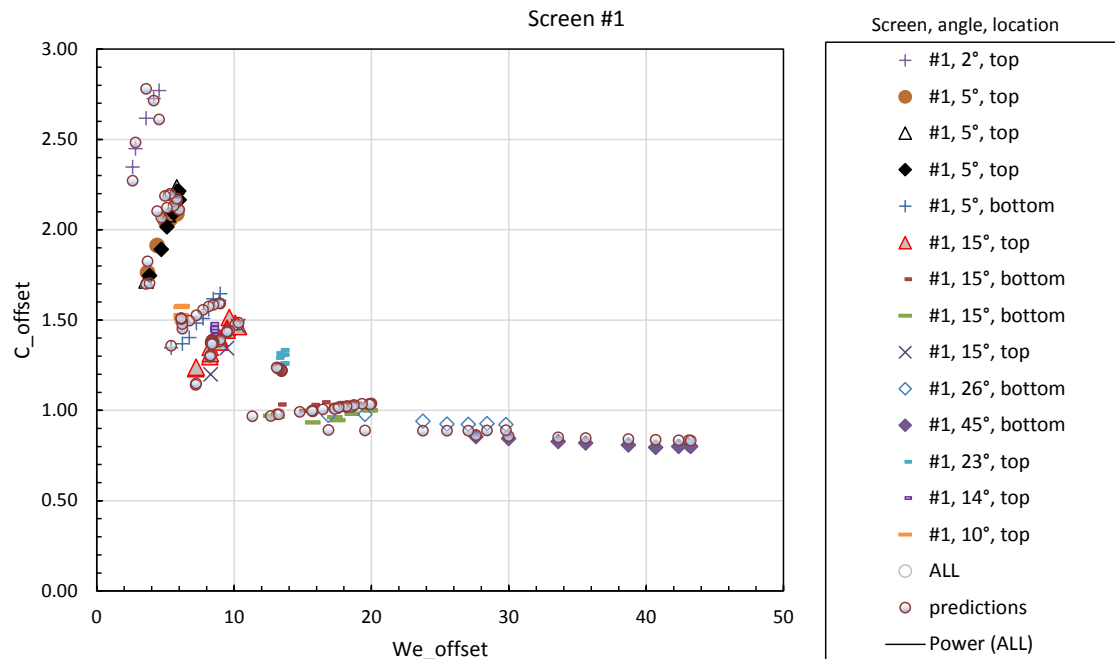
Figure 16. — Predictions of C$_{offset}$ values using Eq. 6 with optimized parameters for screen #1, compared to observed values from screen tests.

Predicted vs. Observed Discharge Coefficients Using "Default" a, b, c, and d Values
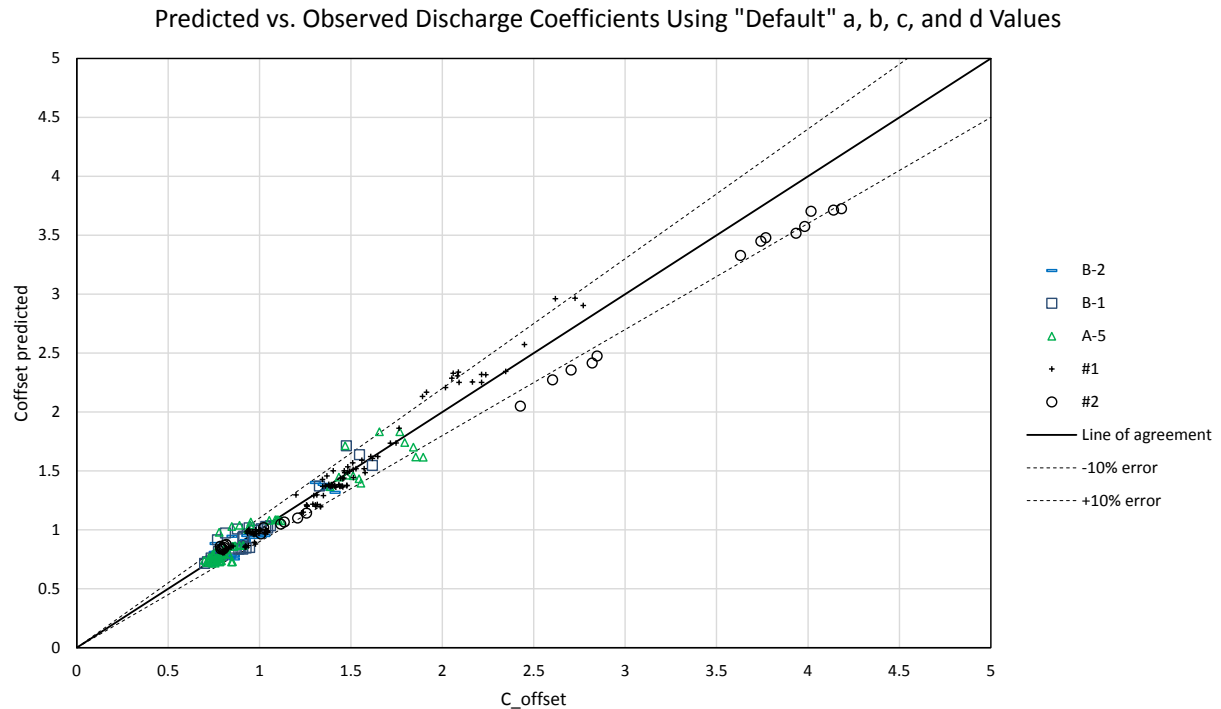
Figure 17. — Predicted and observed discharge coefficients. Compare the scatter of the predictions to Figure 8. Average error is -0.48%. RMS error is 6.94%.

Discussion and Recommendations

To assess the practical importance of the dramatic improvements in the modeling of discharge capacity of Coanda-effect screens, the new discharge coefficient model should be incorporated into the previous software (Wahl 2001) that computes complete flow profiles over a screen structure and the associated flow through the screen. That task remains to be accomplished. The most dramatic changes in discharge capacity will be seen on screens that experience flow at relatively low Froude and Weber numbers, since it is in that range that discharge coefficients are most variable and have the potential to be much larger than the previous models would have predicted. Once this task is accomplished, it would be desirable to update the previous design guide (Wahl 2003) that employed the computer program to demonstrate how changes in structure dimensions and screen properties would affect the total capacity of a screen structure.

In addition to the task described above, three other areas for continued research are apparent at this time.

- Aeration in the receiving chamber beneath a Coanda-effect screen has long been identified as a potential problem with these structures. If aeration is not properly anticipated, water levels in the receiving chamber can become so high that they create backpressure beneath the screen surface, reducing its discharge capacity or lifting screen panels out of place if unsecured.
- The flow skipping behavior that was observed during these tests can be a practical problem when screens have large tilt angles or are installed on steep slopes or in

structures with large drop heights. Testing is needed to develop reliable criteria for determining when the Coanda effect is lost so that flow skipping can be avoided.

- Although Coanda-effect screens are generally self-cleaning, the hydraulic self-cleaning action is not always sufficient to prevent some types of debris from clinging to the screen surface and eventually building up to a point that restricts flow. Research is needed to develop criteria for flow conditions and debris types that lead to a loss of self-cleaning action. It would also be valuable to perform research to develop methods for improving self-cleaning action.

References

Chow, V.T., 1959. *Open-Channel Hydraulics*. McGraw-Hill, New York.

Dzafo, H., Dzaferovic, E., Wahl, T.L., 2017. Use of CFD to analyze edge effects in laboratory testing of Coanda-effect screens. Hydraulic Measurements & Experimental Methods 2017, American Society of Civil Engineers, Durham, NH, July 9-12.

Esmond, S., 2012. Effectiveness of Coanda screens for removal of sediment, nutrients, and metals from urban runoff. 43rd International Erosion Control Association Annual Conference 2012, Las Vegas, Nevada, USA, 26-29 February 2012.

Finch, H.E., and Strong, J.J., 1983. Self-cleaning screen. U.S. Patent No. 4,415,462.

Fontein, F.J., 1965. Some variables influencing sieve-bend performance. *Proceedings, International Chemical Engineers Joint Meeting*, New York.

May, D., 2015. Sediment exclusion from water systems using a Coanda effect device. *International Journal of Hydraulic Engineering,* 4(2): 23-30. DOI: 10.5923/j.ijhe.20150402.01.

Strong, J. J., and Ott, R. F., 1988. Intake screens for small hydro plants. *Hydro Review*, vol. VII, no. V, October 1988.

Wahl, T.L., 2001. Hydraulic performance of Coanda-effect screens". *Journal of Hydraulic Engineering*, 127(6):480-488.

Wahl, T.L., 2003, *Design guidance for Coanda-effect screens*. U.S. Dept. of the Interior, Bureau of Reclamation, Research Report R-03-03. July 2003.

Wahl, T.L., 2013. New testing of Coanda-effect screen capacities. *HydroVision International 2013*, July 23-26, 2013, Denver, CO.

Wahl, T.L., Dzafo, H., and Dzaferovic, E., 2017. Discharge capacity of Coanda-effect screens and the combined influence of gravitational, surface tension, and viscous effects. Hydraulic Measurements & Experimental Methods 2017, American Society of Civil Engineers, Durham, NH, July 9-12.

# Appendix A – Screen Test Plots
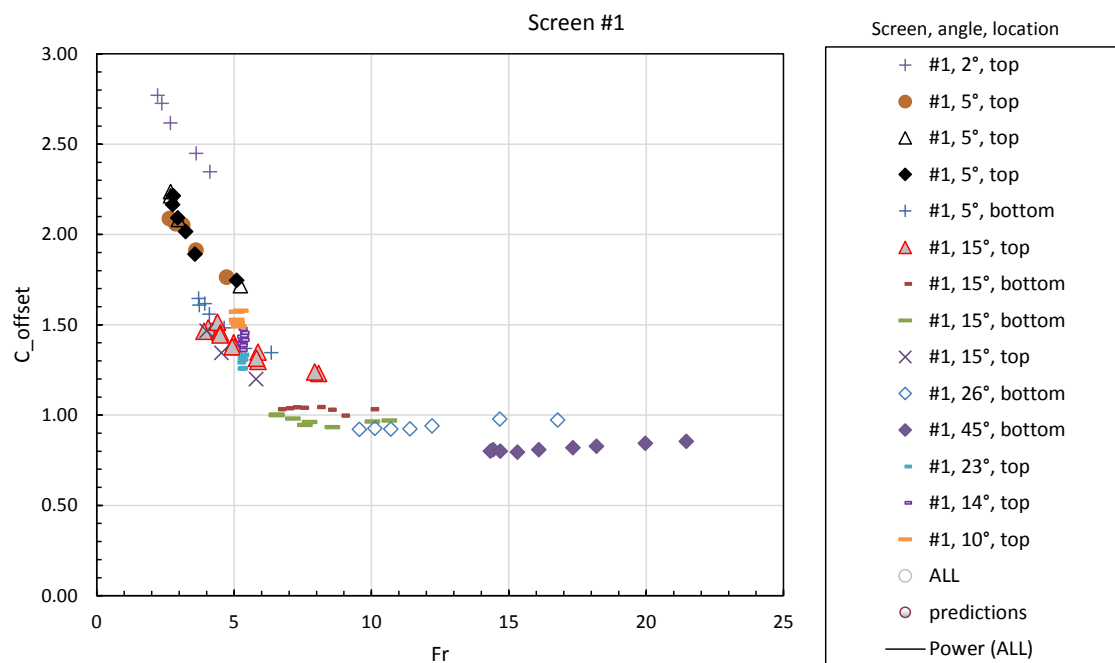
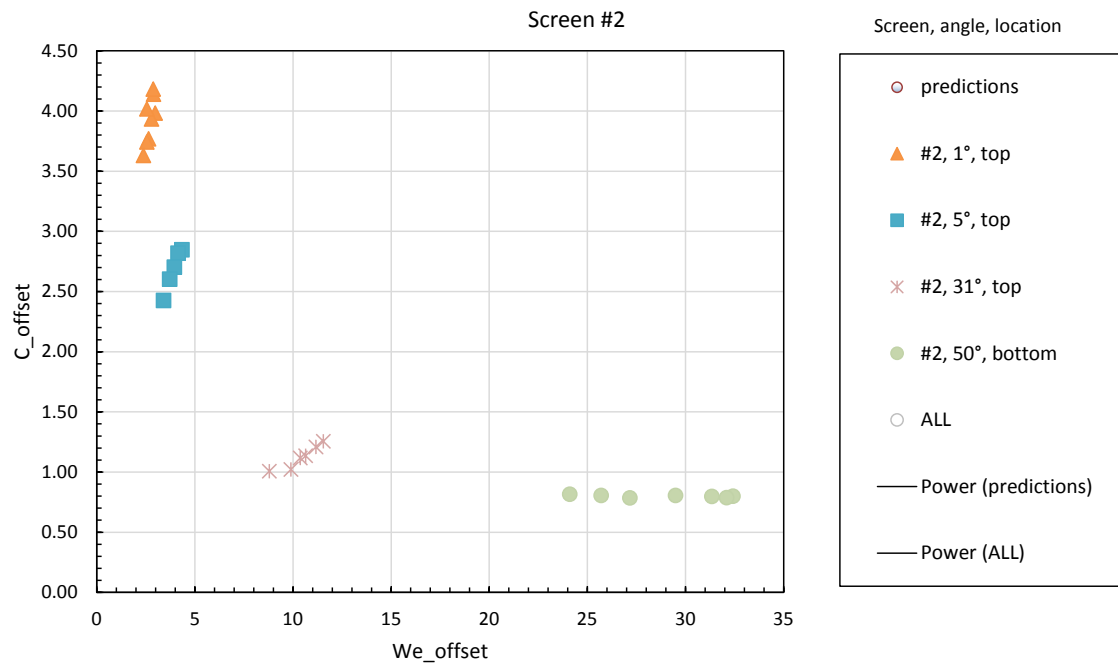Figure A-1. — Screen #1 discharge coeffcient vs. Froude number.
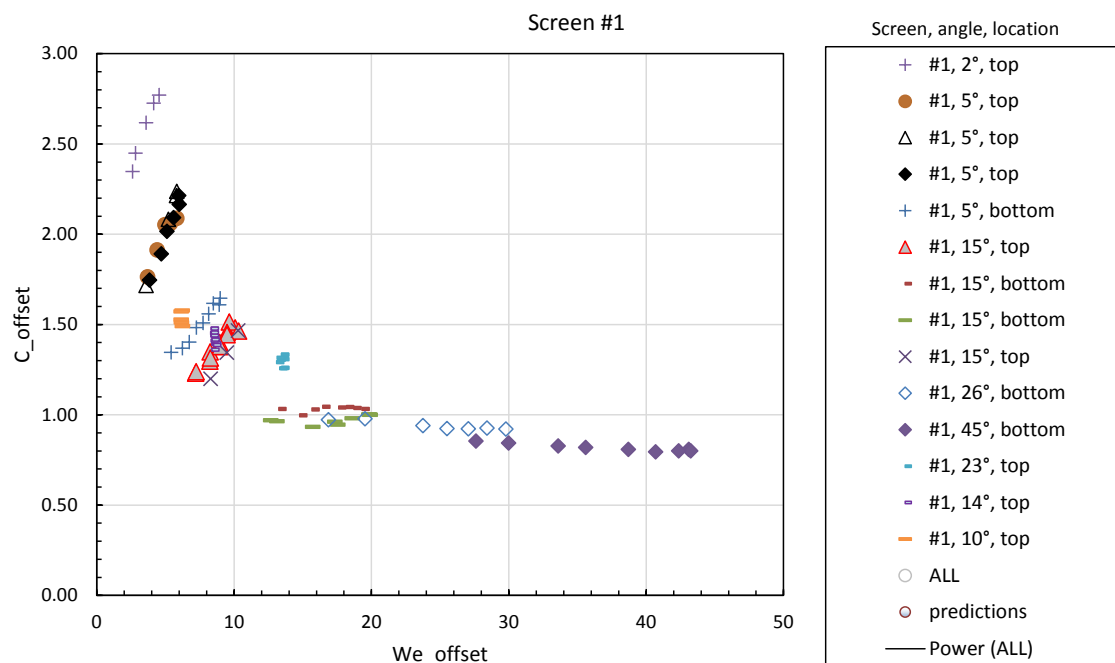
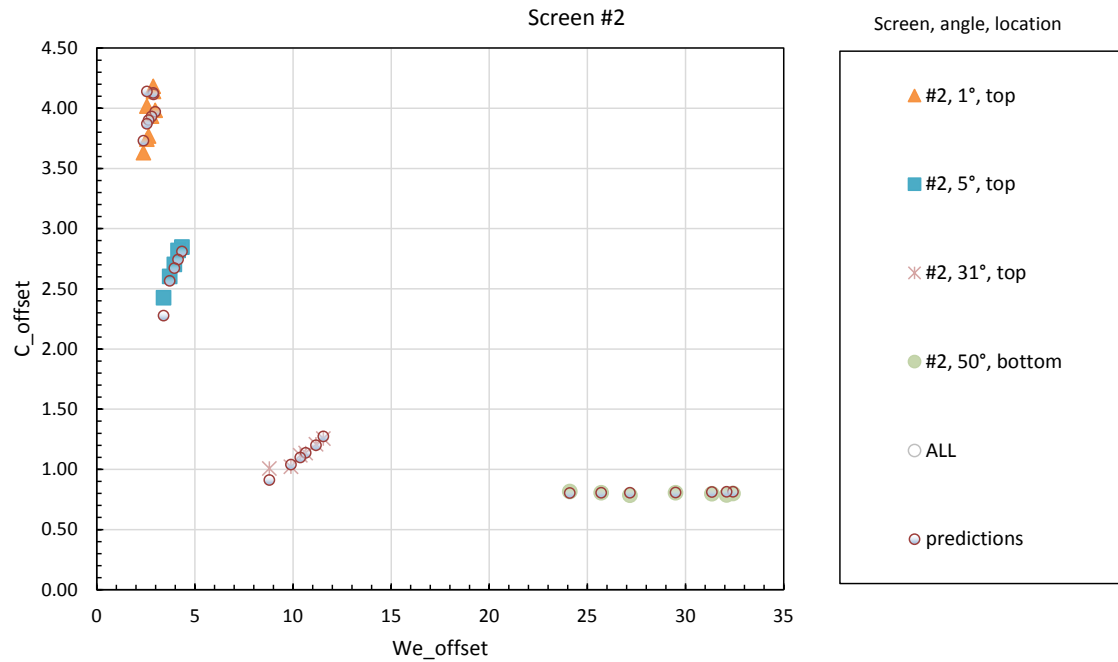Figure A-2. — Screen #1 discharge coefficient vs. Weber number.

A–2
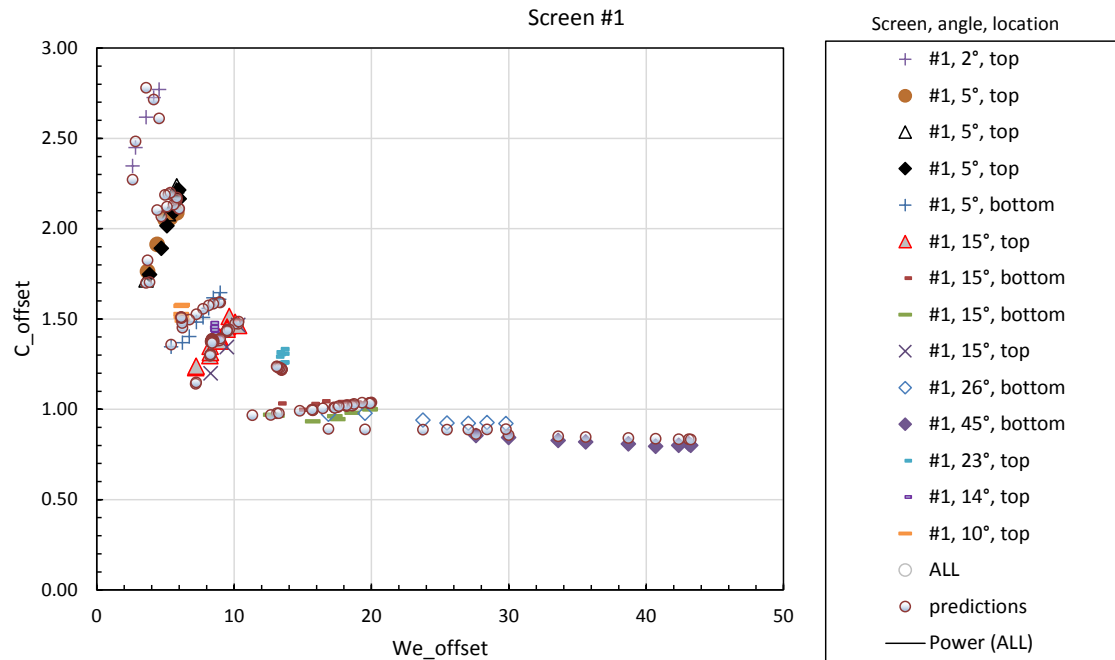
Figure A-3. — Screen #1 discharge coefficient predictions using individually optimized curve-fit parameters in Eq. 6 (Average error = -0.21%. RMS error = 4.54%).
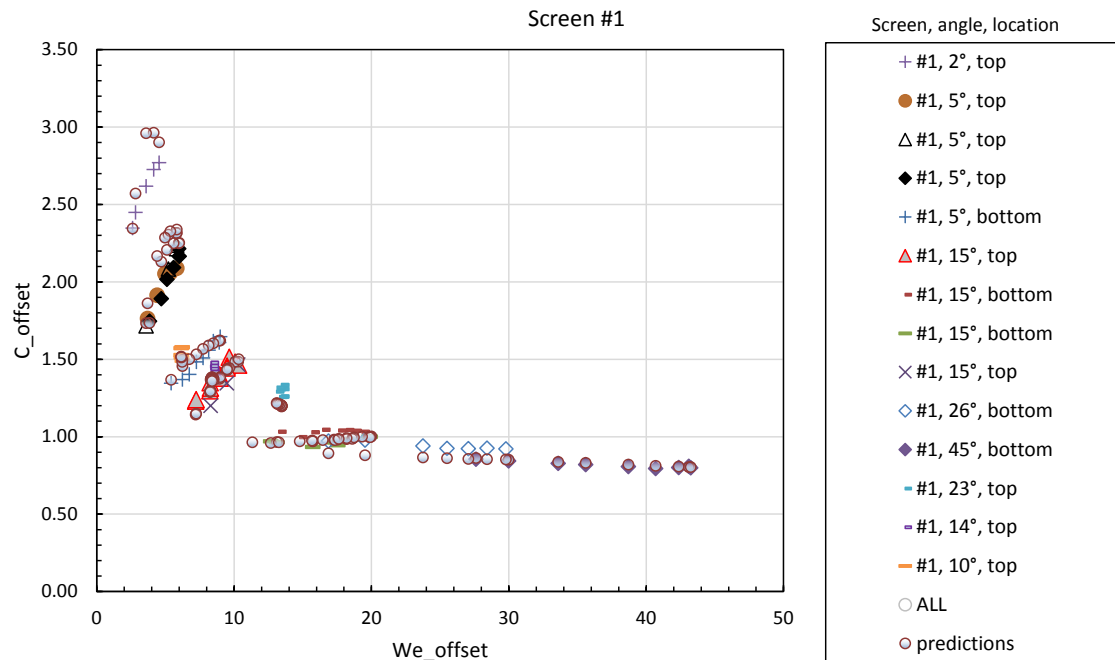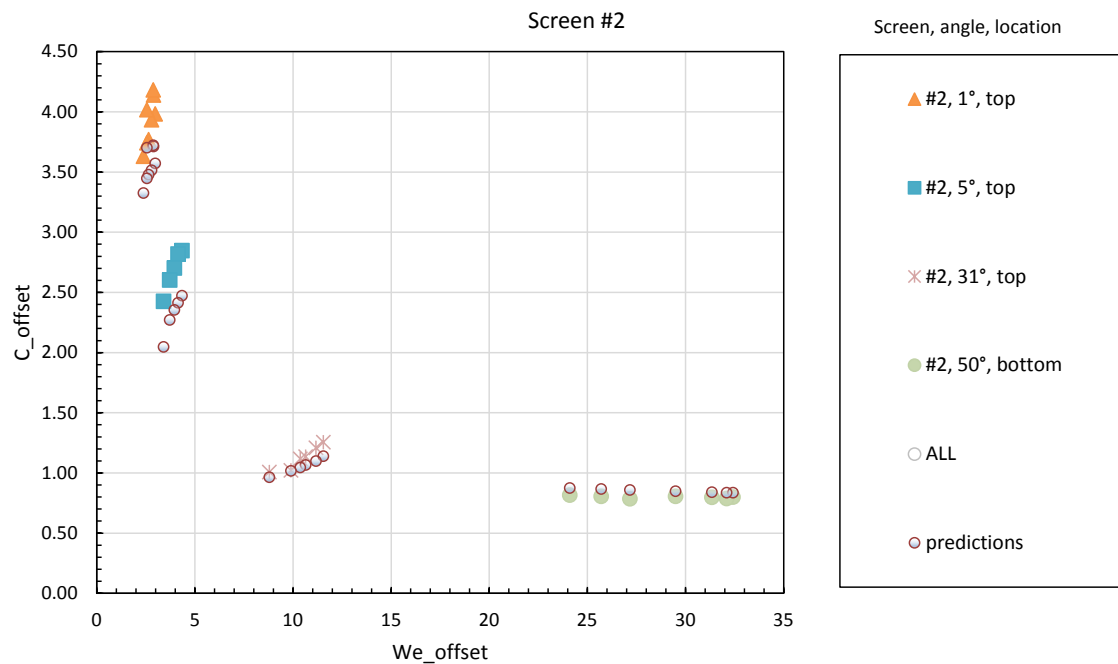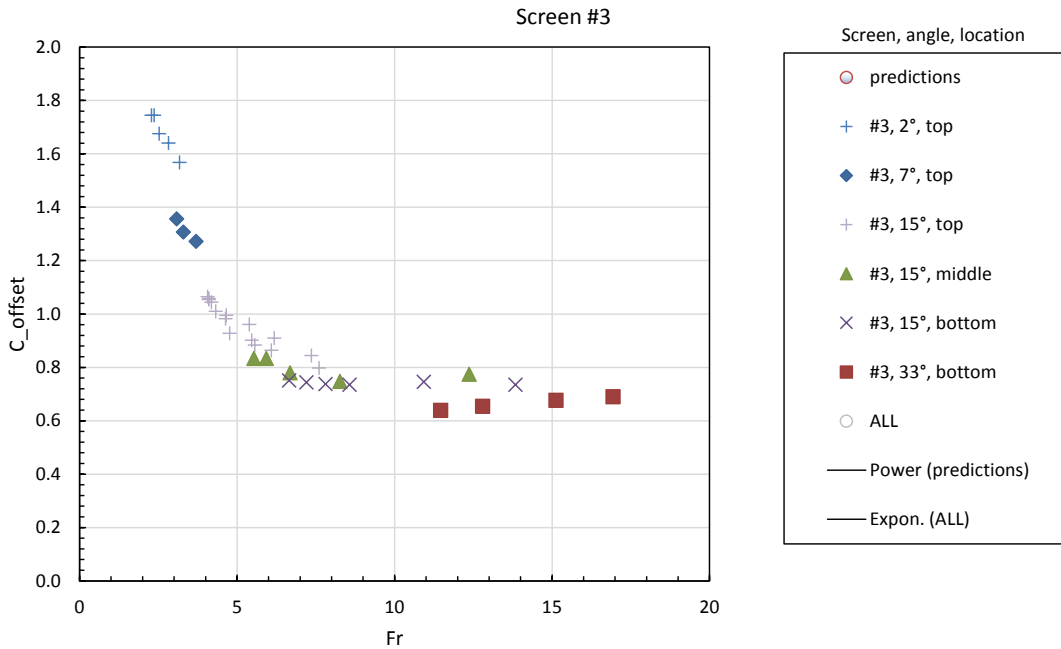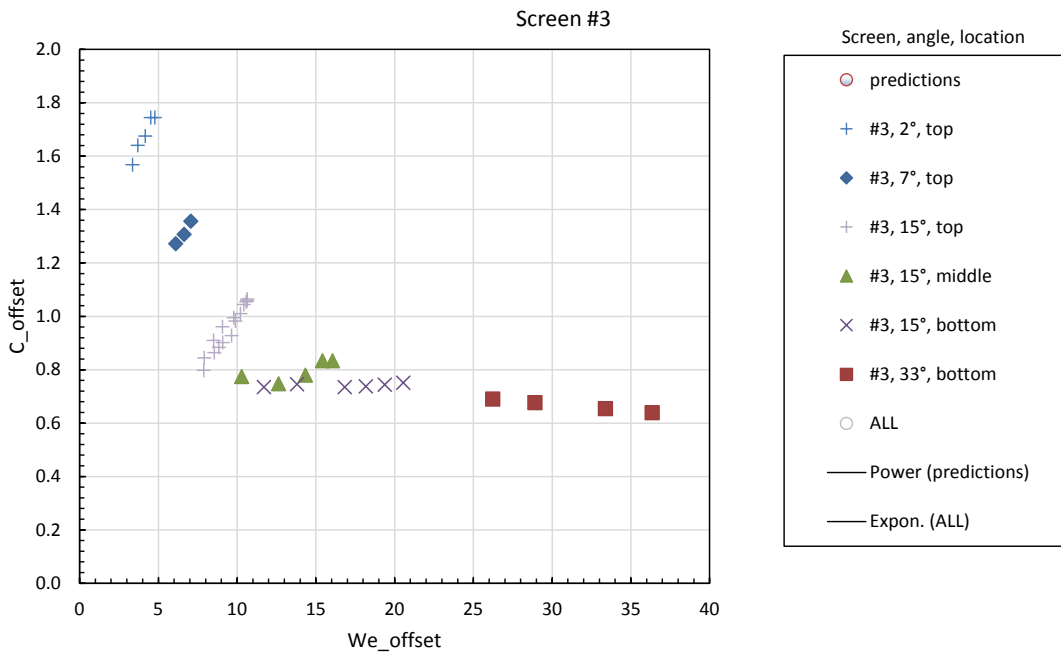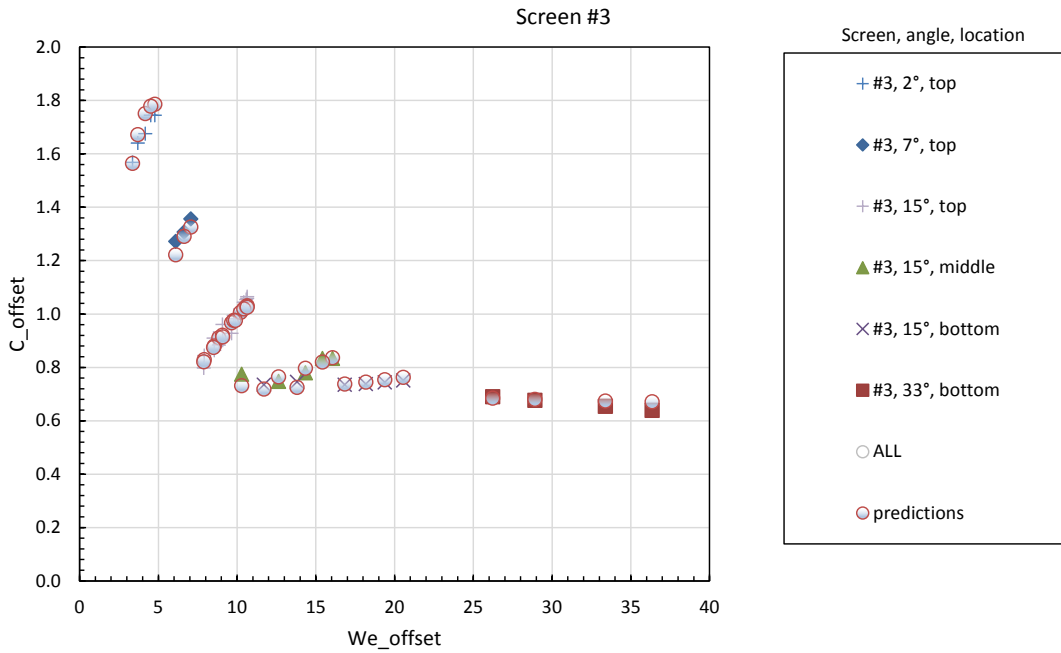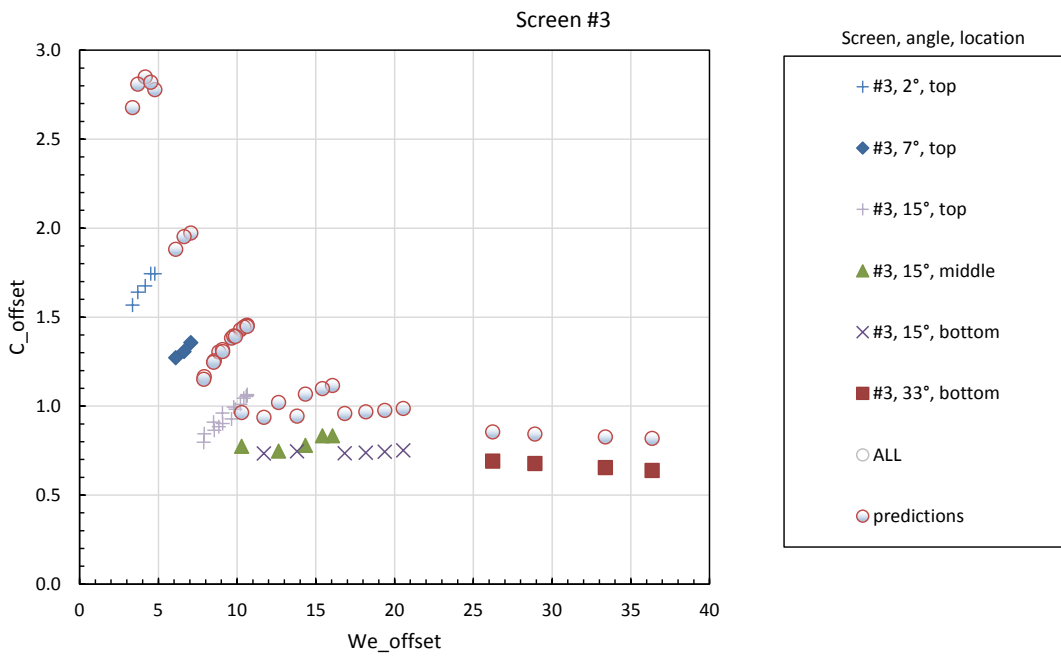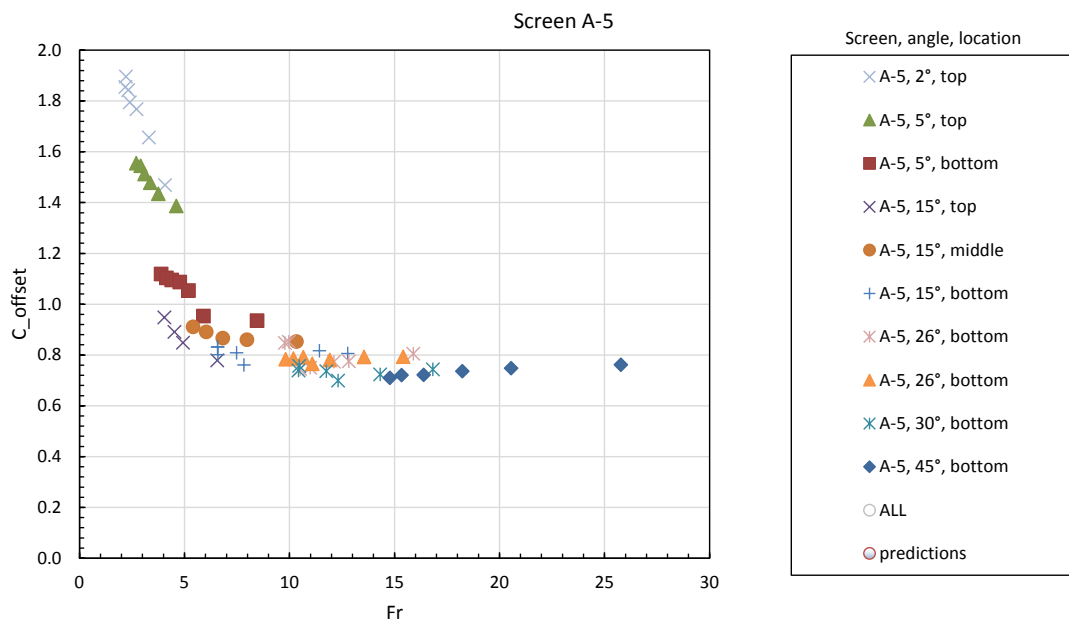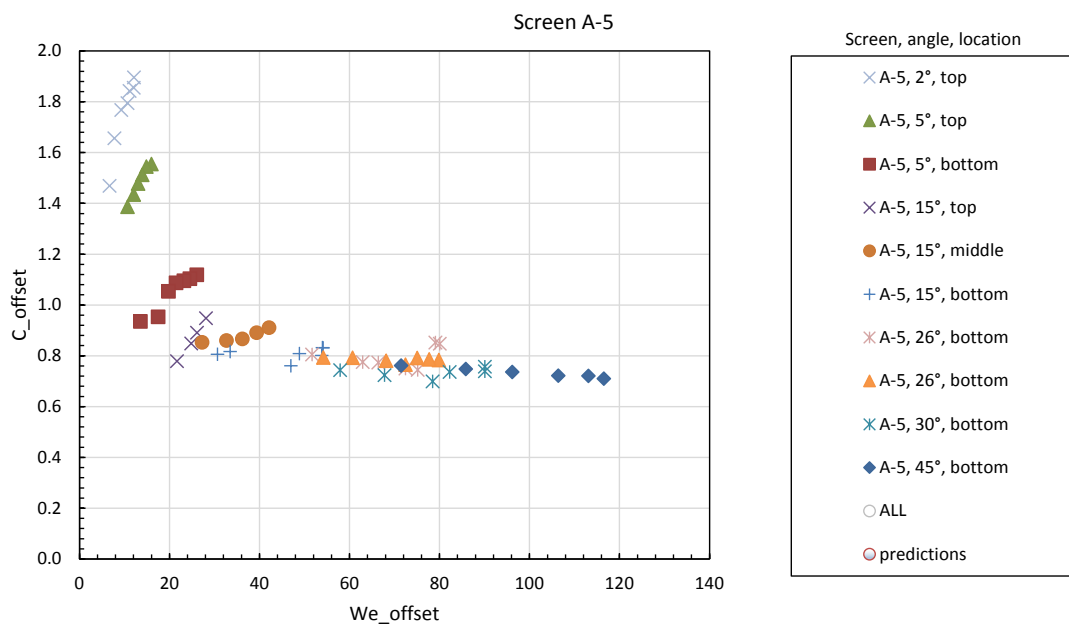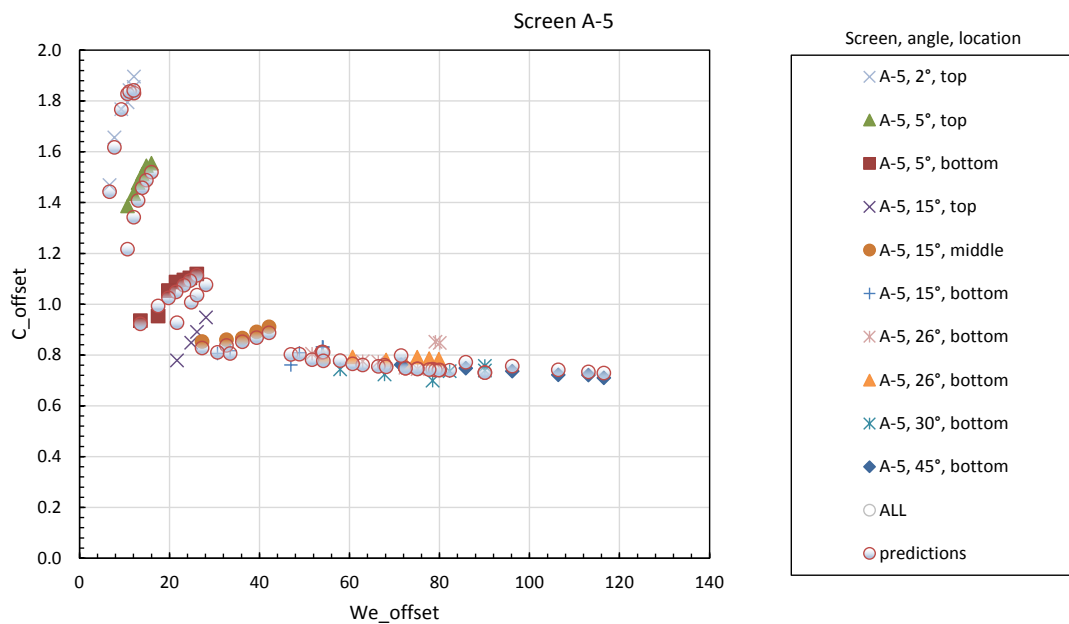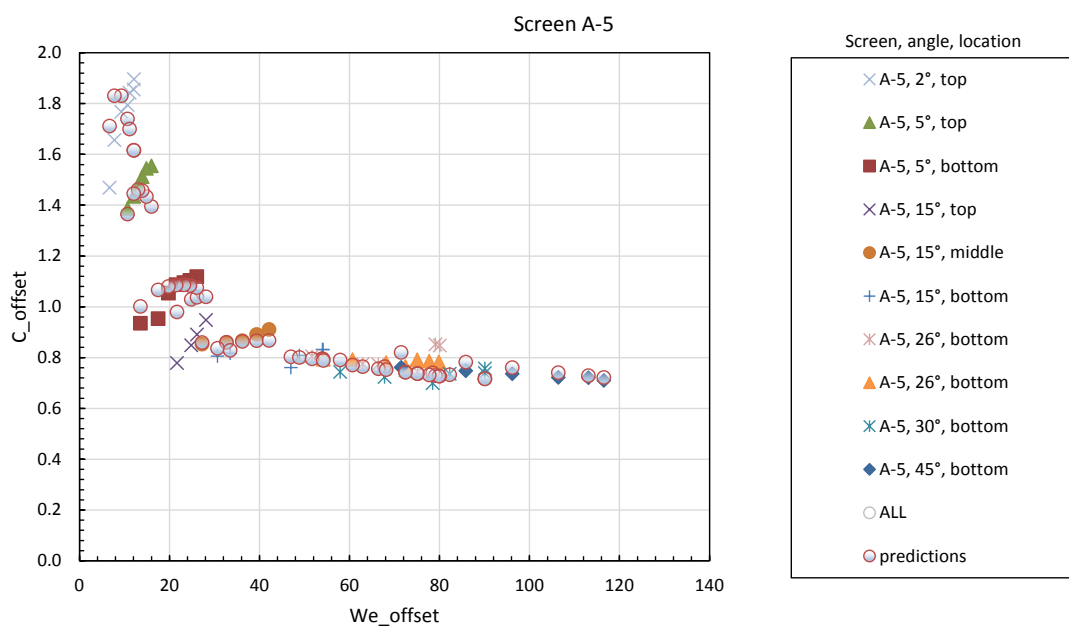

Figure A-4. — Screen #1 discharge coefficient predictions using suggested default curve-fit parameters in Eq. 6 (Average error = -0.32%. RMS error = 5.41%).
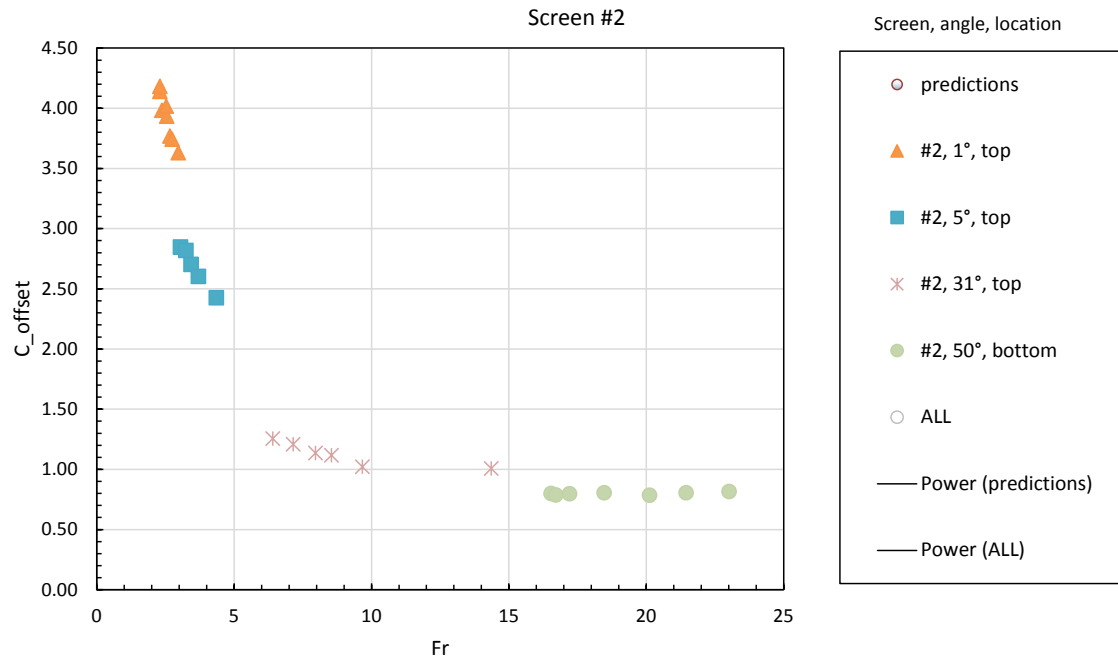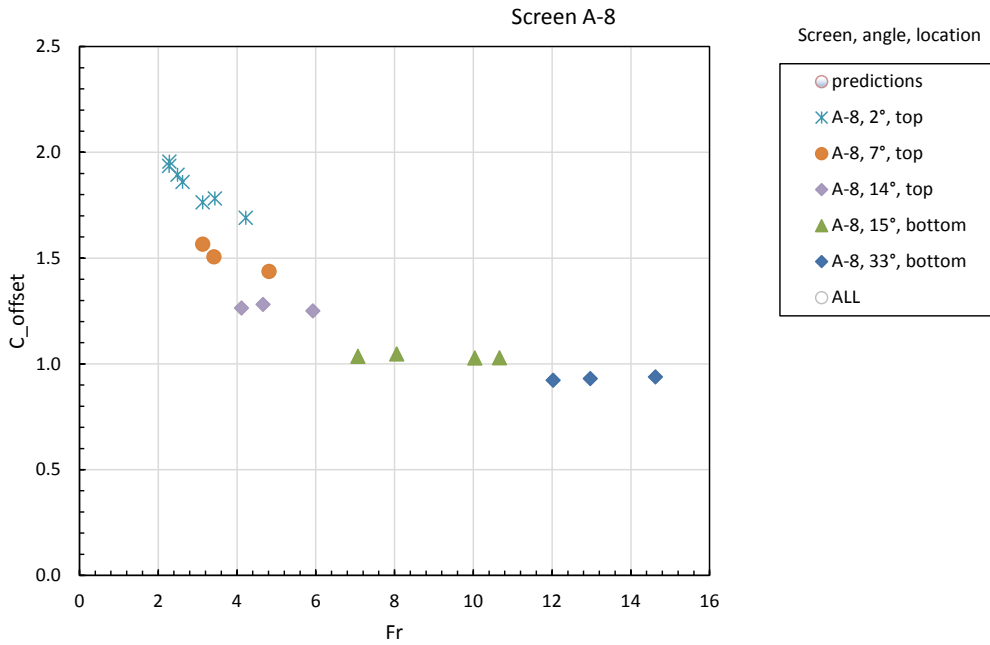
Figure A-5. — Screen #2 discharge coefficient vs. Froude number.
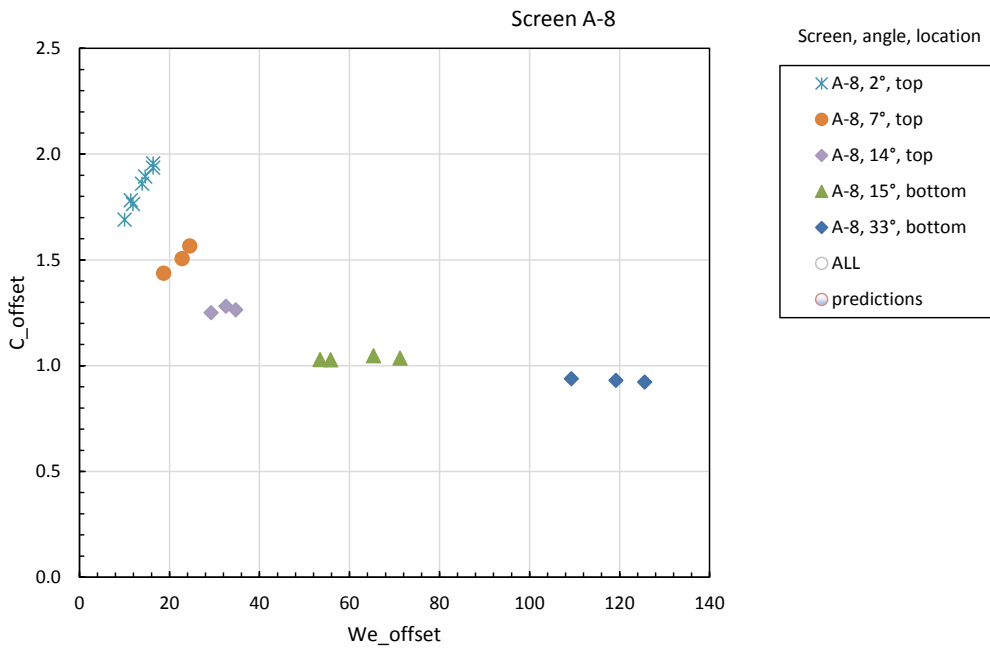

Figure A-6. — Screen #2 discharge coefficient vs. Weber number.

Figure A-7. — Screen #2 discharge coefficient predictions using individually optimized curve-fit parameters in Eq. 6 (Average error = -0.08%. RMS error = 2.90%).

Figure A-8. — Screen #2 discharge coefficient predictions using suggested default curve-fit parameters in Eq. 6 (Average error = -5.11%. RMS error = 9.25%).

Figure A-9. — Screen #3 discharge coefficient vs. Froude number.

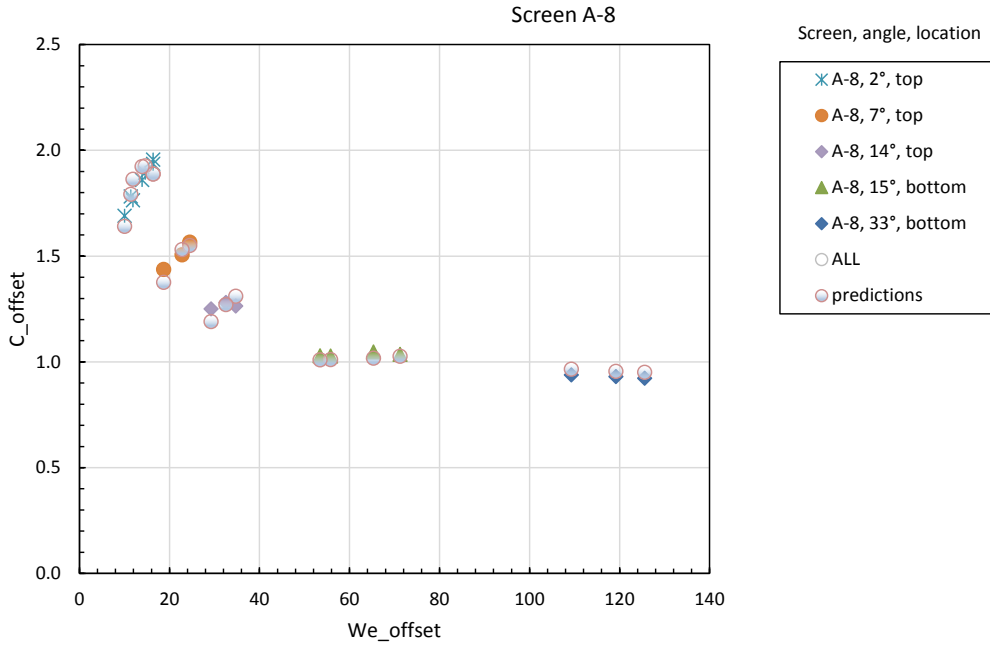Figure A-10. — Screen #3 discharge coefficient vs. Weber number.

Figure A-11. — Screen #3 discharge coefficient predictions using individually optimized curve-fit parameters in Eq. 6 (Average error = -0.07%. RMS error = 2.65%).
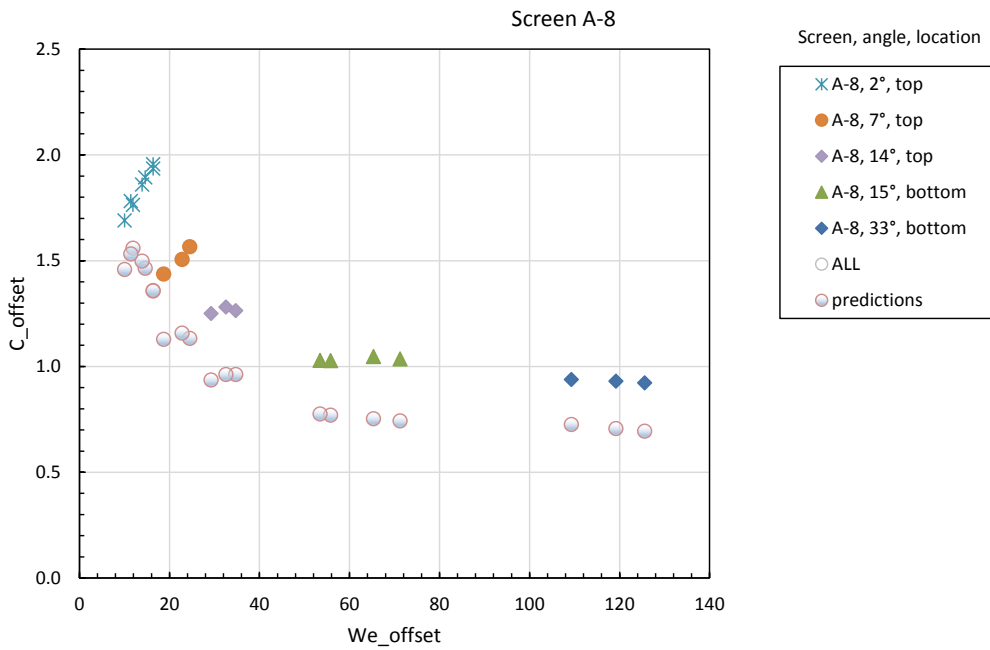

Figure A-12. — Screen #3 discharge coefficient predictions using suggested default curve-fit parameters in Eq. 6 (Average error = 40.43%. RMS error = 42.32%).

Figure A-13. — Screen A-5 discharge coefficient vs. Froude number.

Figure A-14. — Screen A-5 discharge coefficient vs. Weber number.

Figure A-15. — Screen A-5 discharge coefficient predictions using individually optimized curve-fit parameters in Eq. 6 (Average error = -0.35%. RMS error = 5.94%).

Figure A-16. — Screen A-5 discharge coefficient predictions using suggested default curve-fit parameters in Eq. 6 (Average error = 0.23%. RMS error = 7.71%).
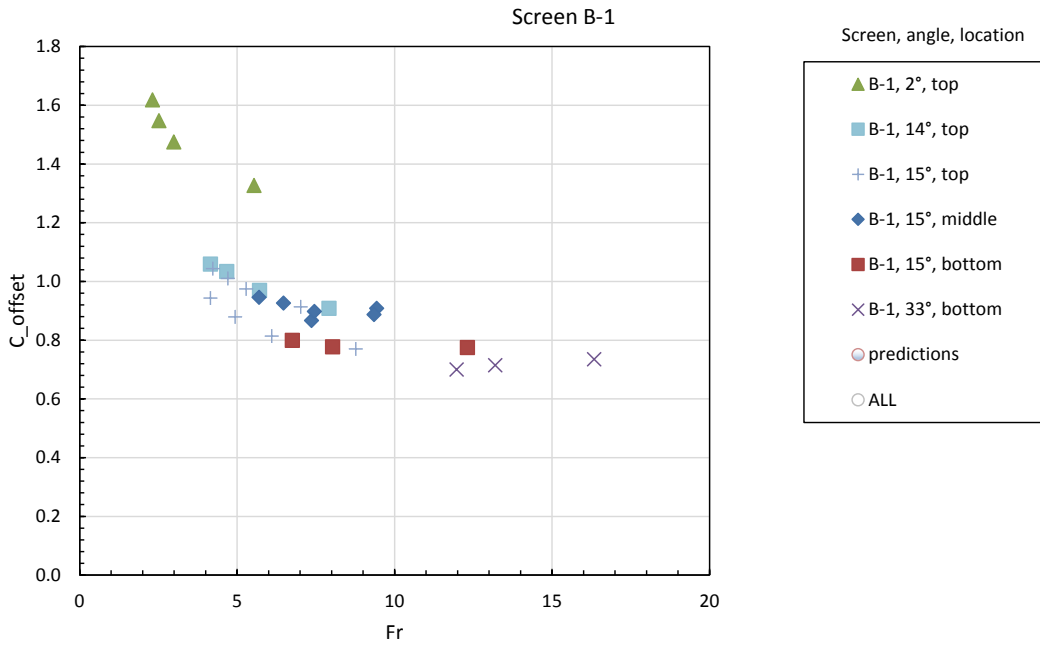
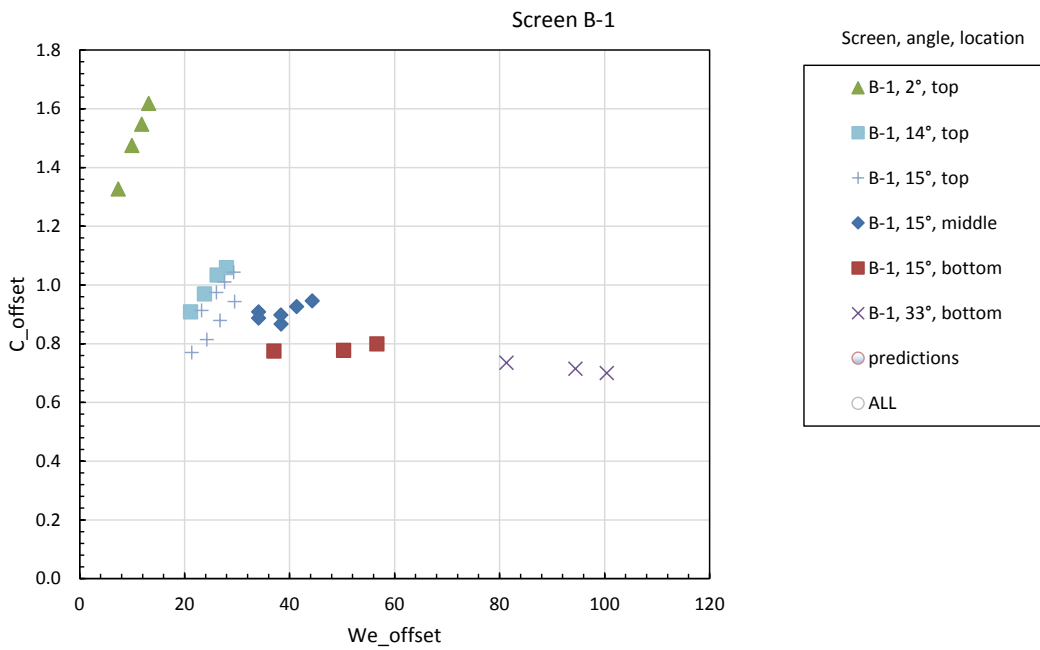Figure A-17. — Screen A-8 discharge coefficient vs. Froude number.

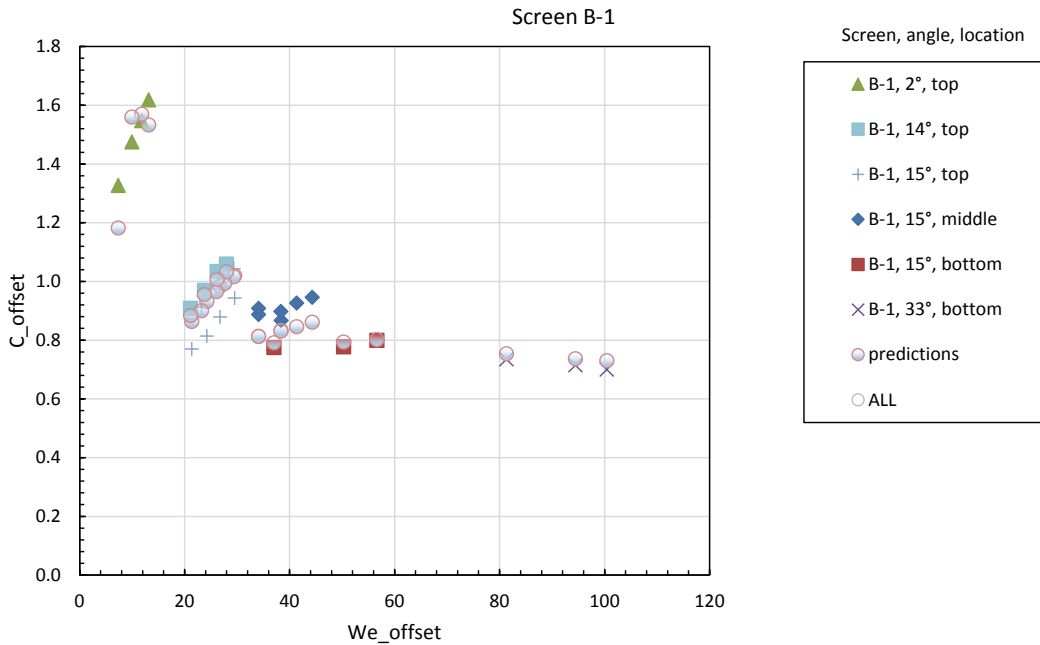Figure A-18. — Screen A-8 discharge coefficient vs. Weber number.

Figure A-19. — Screen A-8 discharge coefficient predictions using individually optimized curve-fit parameters in Eq. 6 (Average error = -0.09%. RMS error = 2.93%).

Figure A-20. — Screen A-8 discharge coefficient predictions using suggested default curve-fit parameters in Eq. 6 (Average error = -23.29%. RMS error = 23.82%).

Figure A-21. — Screen B-1 discharge coefficient vs. Froude number.

Figure A-22. — Screen B-1 discharge coefficient vs. Weber number.

Figure A-23. — Screen B-1 discharge coefficient predictions using individually optimized curve-fit parameters in Eq. 6 (Average error = -0.44%. RMS error = 6.64%).
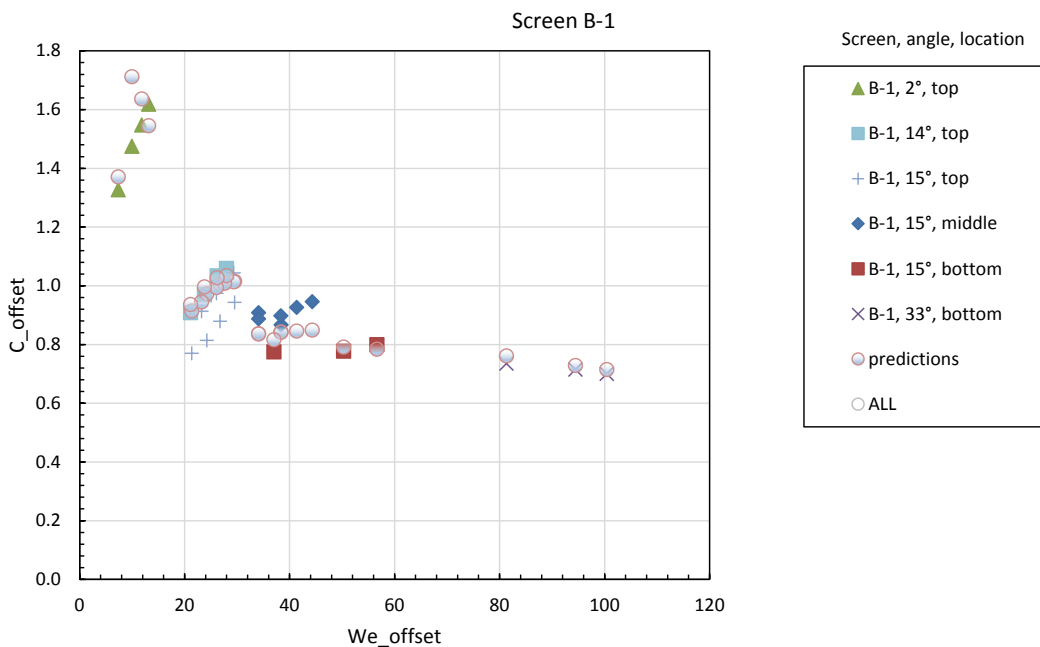

Figure A-24. — Screen B-1 discharge coefficient predictions using suggested default curve-fit parameters in Eq. 6 (Average error = 2.02%. RMS error = 7.90%).
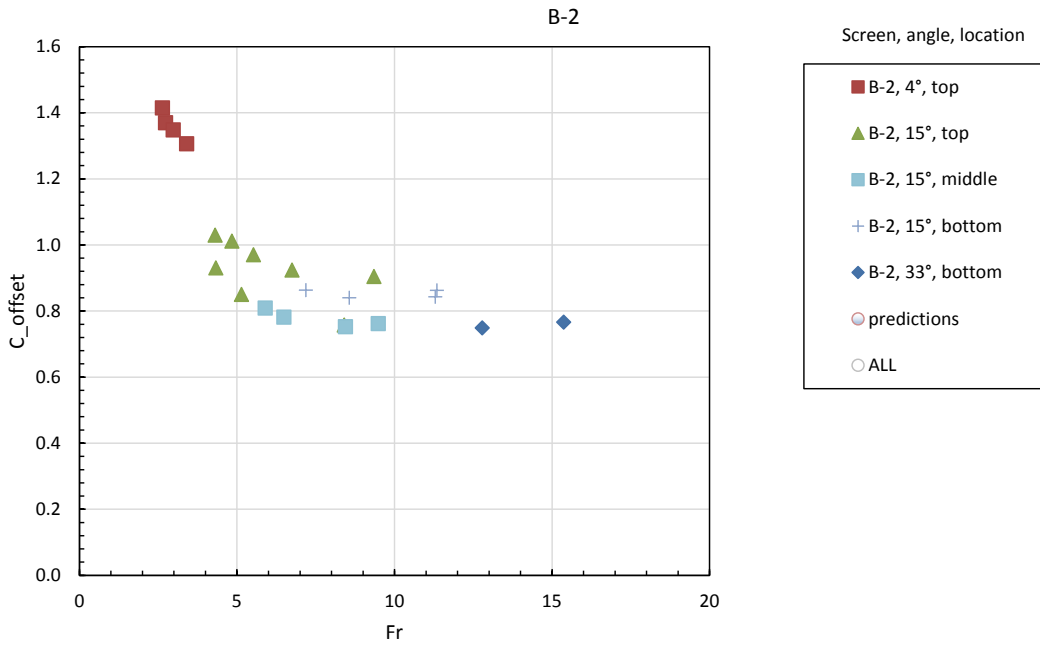
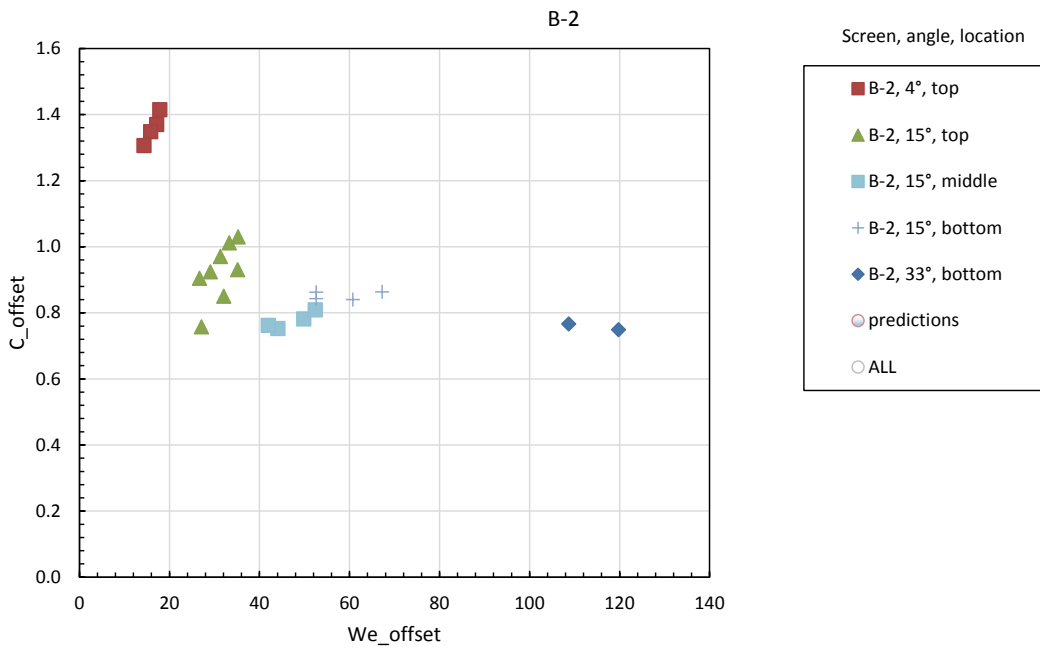Figure A-25. — Screen B-2 discharge coefficient vs. Froude number.

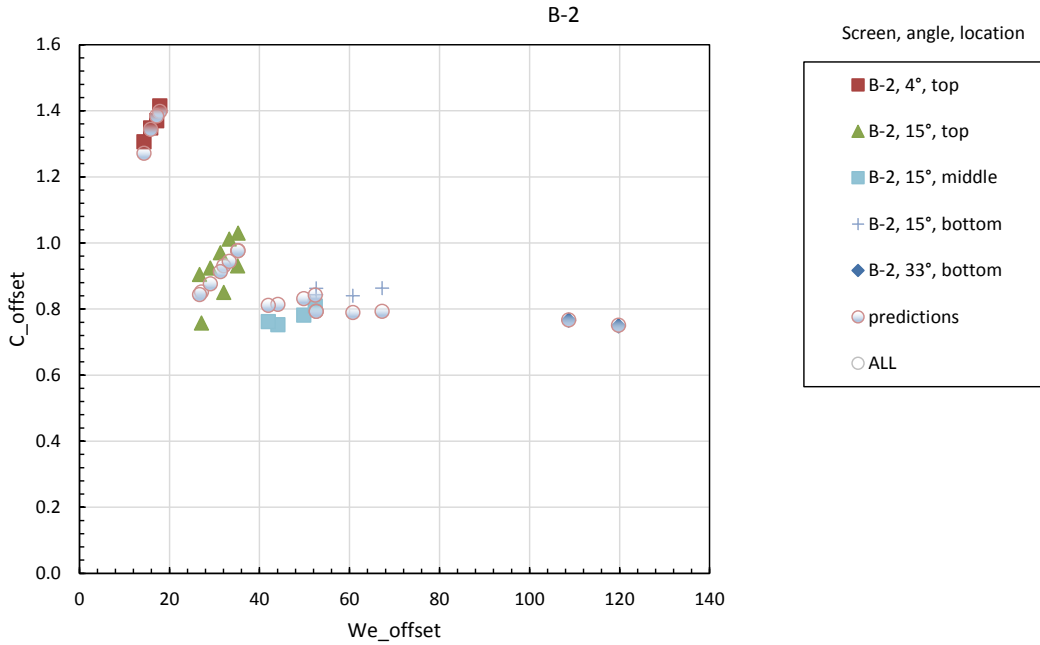Figure A-26. — Screen B-2 discharge coefficient vs. Weber number.

Figure A-27. — Screen B-2 discharge coefficient predictions using individually optimized curve-fit parameters in Eq. 6 (Average error = -0.37%. RMS error = 6.11%).
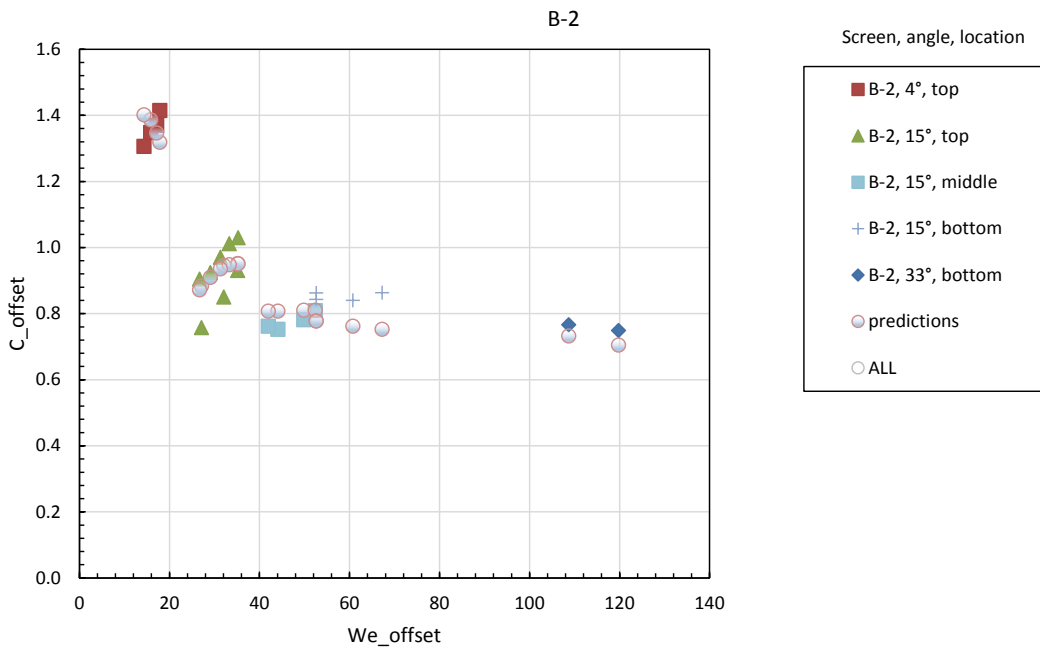

Figure A-28. — Screen B-2 discharge coefficient predictions using suggested default curve-fit parameters in Eq. 6 (Average error = -1.08%. RMS error = 7.42%).

Data Sets that Support the Final Report

- Share Drive folder name and path where data are stored:
  \\bor\do\Team\ENGRLAB\HYDLAB\Project Archives\Wahl\Coanda\CdTests\2016data
- Point of Contact name, email, and phone:
  Tony Wahl, twahl@usbr.gov, 303-445-2155
- Short description of the data:
  Screen test data in Excel spreadsheets, and photographs of test facilities
- Approximate total size of all files: 67 MB